IRS-aided Wireless Powered MEC Systems: TDMA or NOMA for Computation Offloading?

Guangji Chen, Qingqing Wu, *Member, IEEE,* Wen Chen, *Senior Member, IEEE,*
Derrick Wing Kwan Ng, *Fellow, IEEE,* and Lajos Hanzo, *Fellow, IEEE*

***Abstract*—An intelligent reflecting surface (IRS)-aided wireless-powered mobile edge computing (WP-MEC) system is conceived, where each device's computational task can be divided into two parts for local computing and offloading to mobile edge computing (MEC) servers, respectively. Both time division multiple access (TDMA) and non-orthogonal multiple access (NOMA) schemes are considered for uplink (UL) offloading. To fully unleash the potential benefits of the IRS, employing multiple IRS beamforming (BF) patterns/vectors in the considered operating frame to create time-selectivity channels, i.e., dynamic IRS BF (DIBF), is in principle possible at the cost of additional signaling overhead. To strike a balance between the system performance and associated signalling overhead, we propose three cases of DIBF configurations based on the maximum number of IRS reconfiguration times. The degree-of-freedom provided by the IRS may introduce different impacts on the TDMA and NOMA-based UL offloading schemes. Thus, it is still fundamentally unknown which multiple access scheme is superior for MEC UL offloading by considering the impact of the IRS. To answer this question, we provide a comprehensively theoretical performance comparison for the TDMA and NOMA-based offloading schemes under the three cases of DIBF configurations by characterizing their achievable computation rate. Analytical results demonstrate that offloading adopting TDMA can achieve the same computation rate as that of NOMA, when all the devices share the same IRS BF vector during the UL offloading. By contrast, computation offloading exploiting TDMA outperforms NOMA, when the IRS BF vector can be flexibly adapted for UL offloading. Then, we propose computationally efficient algorithms by invoking alternating optimization for solving their associated computation rate maximization problems. Our numerical results demonstrate the significant performance gains achieved by the proposed designs over various benchmark schemes and also unveil that the optimal time allocated to downlink wireless power transfer can be effectively reduced with the aid of IRSs, which is beneficial for both the system's spectral efficiency and its energy efficiency.**

***Index Terms*—IRS, wireless powered mobile edge computing, dynamic beamforming, NOMA, TDMA.**

The work of Qingqing Wu was supported by the FDCT under Grant0119/2020/A3. The work of Wen Chen was supported by National key project 2020YFB1807700 and 2018YFB1801102, by Shanghai Kewei 20JC1416502 and 22JC1404000, and NSFC 62071296. The work of Derrick Wing Kwan Ng was supported by the Australian Research Council's Discovery Project (DP210102169). The work of Lajos Hanzo was supported by the Engineering and Physical Sciences Research Council projects EP/W016605/1 and EP/P003990/1 (COALESCE) as well as of the European Research Council's Advanced Fellow Grant QuantCom (Grant No. 789028). (Corresponding author: Qingqing Wu.)

G. Chen and Q. Wu are with the State Key Laboratory of Internet of Things for Smart City, University of Macau, Macao 999078, China (e-mail: guangjichen@um.edu.mo; qingqingwu@um.edu.mo). W. Chen is with the Department of Electronic Engineering, Shanghai Institute of Advanced Communications and Data Sciences, Shanghai Jiao Tong University, Minhang 200240, China (e-mail: wenchen@sjtu.edu.cn). Derrick Wing Kwan Ng is with the School of Electrical Engineering and Telecommunications, UNSW Sydney, Sydney, NSW 2052, Australia (e-mail: w.k.ng@unsw.edu.au). L. Hanzo is with the Department of Electronics and Computer Science, University of Southampton, Southampton SO17 1BJ, U.K. (e-mail: lh@ecs.soton.ac.uk). Part of the paper has been presented at the IEEE WCNC Workshops 2022 [1]

I. Introduction

With the rapid development of popular Internet-of-Everything (IoE) technologies, the unprecedented proliferation of mobile sensors, electronic tablets, and wearable devices is set to continue in support of smart transportation, smart homes, and smart cities [2]. For realizing the IoE, next generation wireless networks are expected to support massive number of connections and to accommodate huge data traffic. As such, superior multiple access (MA) schemes are required to attain high spectral efficiency (SE) for a massive number of IoE devices in next generation wireless networks [3]. Recently, it has been shown that non-orthogonal multiple access (NOMA) is capable of improving the SE by allowing multiple users to simultaneously access the same spectrum. Therefore, NOMA has been recognized as one of the key technologies in next generation wireless networks [3].

On the other hand, an IoE device is often equipped with a low-performance processor and limited battery capacity, given their small practical size and cost constraints. In particular, the emerging applications, such as unmanned driving and automatic navigation, generally rely on the execution of low-latency and computation-intensive tasks, thus imposing new challenges on IoE devices [4]. As a remedy, by incorporating radio frequency (RF)-based wireless-power transmission (WPT) and mobile edge computing (MEC), wireless-powered MEC (WP-MEC) becomes a promising solution for granting self-sustainability and high computational capabilities to IoE systems [5]–[14]. Specifically, RF-based WPT enables energy harvesting (EH) from RF signals and it is capable of prolonging the battery recharge-period of devices [14]–[16]. To improve the computational capabilities for IoE systems, the MEC technology enables IoE devices to offload their tasks to nearby MEC servers in real time, which can compute their tasks remotely and timely [4].

To enhance the computational efficiency of traditional WP-MEC systems, sophisticated resource allocation designs relying on optimization objectives, such as computation rate maximization [6]–[8], energy consumption [10]–[12], and latency minimization [13], etc, have been proposed. For instance, in [5], the WP-MEC framework was proposed for a single-user setup, where the probability of successfully processing a given amount of data was maximized subject to both end-to-end latency and EH constraints. In general, MEC supports a pair of basic operational modes, namely binary and partial offloading modes [5]–[9]. Specifically, for the partial offloading mode, the computational task can be divided into two parts for partial local computing and offloading, respectively, while for the binary offloading mode, the computational task cannot be partitioned, hence it is either executed at the local device or offloaded

to MEC servers [9]. Based on the concept of binary and partial offloading modes, the corresponding computation rate maximization problem was investigated in [6]–[8] for a multi-user setup, where time division multiple access (TDMA) was adopted for uplink (UL) offloading. As a further advance, the superiority of employing NOMA over TDMA in WP-MEC systems was quantified in terms of its energy efficiency improvement [10]–[12] and latency reduction [13]. Therefore, NOMA is regarded as an attractive scheme for UL offloading in traditional WP-MEC systems.

However, the efficiency of both the downlink (DL) WPT and UL offloading may become severely degraded by the wireless channel attenuation between transceivers, which thus fundamentally limits the performance of WP-MEC systems. With the goal of tacking this issue, the authors of [14] exploited the multiple-input multiple-output (MIMO) technique for improving the WPT efficiency and studied the corresponding energy consumption minimization problem. Although the massive MIMO technology can considerably improve the efficiency of both WPT and offloading by exploiting the huge beamforming (BF) gain [17], [18], the associated high hardware cost and energy consumption are still grave obstacles in the way of its practical implementation. Recently, intelligent reflecting surfaces (IRSs) have been proposed as a cost-effective technology for improving the spectral efficiency and energy efficiency of next generation wireless networks [19]–[22]. Specifically, an IRS is a planar array comprised of a large number of low-cost passive reflecting elements, which can reflect incident signals and intelligently adapt their phase shifts according to the real-time channel conditions [20]. As such, IRSs are capable of reconfiguring the wireless propagation environment for achieving e.g., signal enhancement and/or interference suppression. In particular, the fundamental squared-power gain of IRSs was originally unveiled in [23], which then inspired intensive research interests in investigating various IRS-aided wireless systems.

The new research paradigms of IRS-aided wireless information transmission (WIT), WPT, and MEC have been extensively studied in the literature. For IRS-aided WIT systems, joint passive BF at IRSs and active BF at base stations (BSs) was designed either for minimizing the transmit power of BSs or for maximizing the system capacity, e.g., [23]–[28]. As a further practical development, the analysis and optimization of IRS-aided wireless communications were studied by considering both discrete phase shifts [29], [30] and amplitude-dependent phase shifts [31]. In addition to exploiting IRSs for improving the WIT performance, the IRS technology is also appealing for WPT in IoE applications, thanks to its beneficial passive BF gain [32]. Specifically, a promising line of research focused on passive BF design for simultaneous wireless information and power transfer (SWIPT) systems [33]–[35]. Another line of research investigated IRS-aided wireless powered communication networks (WPCNs), where the devices first harvest energy in the DL and then transmit information in the UL [36]–[39]. However, in traditional MEC systems, the task offloading efficiency may not be satisfactory due to the harsh propagation conditions of the wireless links. To address this issue, the authors of [40], [41] exploited the IRS technology for improving the offloading efficiency of MEC systems by studying the associated computation rate maximization and offloading latency minimization problems, respectively.

Given the aforementioned benefits of the IRS technique, its employment in WP-MEC systems is attractive for realizing IoE, since both the efficiency of DL WPT and UL offloading can potentially be improved. Despite the fruitful results of the aforementioned research works on the topic of IRS-aided MEC/WP-MEC, one fundamental issue still remains unsolved. It is still unknown whether NOMA outperforms TDMA regarding the computation rate in an IRS-aided WP-MEC system. Thanks to the adaptive BF capability of the IRS, favourable time-varing channels can be proactively generated by properly designing IRS BF vectors over different time slots, which facilitates the exploitation of the multiuser diversity over time. For the TDMA-based offloading scheme, each device is capable of employing its dedicated IRS BF vector/pattern for enhancing its channel quality by harnessing the favorable time-selectivity wireless channels created by the IRS. It is generally believed that the time-varying channels introduced by the IRS have significantly positive effects on the TDMA-based offloading scheme. Regarding the NOMA-based offloading scheme, it is not clear whether it can be benefited by the time-varying channels. Different from previous works considering a conventional MEC/WP-MEC system [10]–[13], the conclusion on TDMA versus NOMA in our considered system needs to be reexamined by carefully characterizing and analyzing the impact of the IRS. This knowledge-gap motivates us to investigate the achievable computation rate in IRS-aided WP-MEC scenarios by considering the interplay between IRSs and MA schemes. To characterize the achievable computation rate of IRS-aided WP-MEC systems, the main challenges we identify are as follows: 1) the specific IRS configuration required for reaping the potential benefits of WP-MEC systems has to be identified; 2) the design of IRS BF and resource allocation for WP-MEC systems is generally intractable.

To address the above issues, this paper investigates the achievable computation rate maximization problems of IRS-aided WP-MEC systems by considering two types of offloading schemes, i.e., TDMA and NOMA. Specifically, we focus our attention on a typical setup, where a hybrid access point (HAP) is exploited both as the energy transmitter and the MEC server. Moreover, an IRS is deployed for enhancing the efficiency of both DL WPT and UL offloading. Our main contributions are summarized as follows:

- We propose an offloading framework for investigating the performance of IRS-aided WP-MEC systems, where three different levels of dynamic IRS BF (DIBF) schemes are considered: **Case 1**: both DL WPT and UL offloading share the same IRS BF vector; **Case 2**: two different IRS BF vectors are exploited for DL WPT and UL offloading, respectively; **Case 3**: the IRS BF vectors can be further adapted for UL offloading with respect to each individual device. Under this framework, we formulate the corresponding computation rate maximization problems by jointly optimizing the resource allocation and the IRS BF for the aforementioned three cases.
- We analytically show that appropriately adjusting the IRS BF vectors for UL offloading is capable of improving the computation rate of TDMA, while it is not beneficial for that of NOMA. By analyzing the relationship between the

computation rate maximization problems of TDMA and NOMA, we prove that the computation rate achieved by TDMA is the same as that by NOMA for both **Case 1** and **Case 2**. By contrast, since TDMA-based IRS-aided WP-MEC systems are capable of benefiting from varying the IRS BF vectors in the UL offloading stage, the computation rate of TDMA exceeds that of NOMA for **Case 3**.

- To gain insights into the beneficial effect of IRSs on WP-MEC systems, we first consider a single-user setup, where we derive a threshold-based UL offloading activation condition. Specifically, we demonstrate that UL offloading is activated if and only if (iff) the transmit power of the HAP is above a certain threshold and increasing the number of IRS elements is capable of reducing the threshold. For the more general multi-user setup, we develop an efficient alternating optimization (AO) algorithm for solving the resultant problems, where the resource allocation and the IRS BF design subproblems are solved alternatingly.
- Our numerical results show that the proposed IRS-aided WP-MEC designs are capable of substantially improving the computation rate compared to the benchmark schemes. It is also found that exploiting IRSs not only increases the total energy harvested via DL WPT, but also leaves more time available for UL offloading, which unveils a further benefit of IRSs for WP-MEC systems. Moreover, the computation rate of **Case 3** significantly exceeds that of **Case 1** and **Case 2**, while the performance loss of **Case 1** compared to **Case 2** is negligible. The results imply that the associated signaling overhead can be reduced by opting for **Case 1** instead of **Case 2** at the cost of a modest performance erosion.

The rest of this paper is organized as follows. Section II presents our system model and problem formulations. Section III provides the theoretical performance comparison of NOMA and TDMA-based UL offloading. Section IV focuses on studying the impact of IRSs on the UL offloading activation condition. Section V proposes computationally efficient algorithms for solving the formulated problems for the different scenarios. Section VI provides numerical results for evaluating the proposed designs. Finally, Section VII concludes the paper.

Notations: $\mathbb{C}^{x\times y}$ stands for the set of complex $x \times y$ matrix. $\mathbb{Z}^+$ represents the set of positive number. For a complex-valued vector $\mathbf{a}$, the n-th entry is denoted by $[\mathbf{a}]_n$, $\mathbf{a}^H$ and $\mathbf{a}^T$ denote Hermitian transpose and transpose, respectively, $\mathrm{diag}\,(\mathbf{a})$ denotes a diagonal matrix with each diagonal entry being the corresponding entry in $\mathbf{a}$. The real part and the phase of a complex number c are denoted by $\mathrm{Re}\,(c)$ and $\arg\,(c)$, respectively. $\mathcal{O}\,(\cdot)$ is the big-O computational complexity notation.

II. System Models and Problem Formulations

A. System Model

As shown in Fig. 1, an IRS-aided WP-MEC system is considered, which consists of a HAP, an IRS[1], and K wireless-powered devices. In particular, a MEC server and an RF energy transmitter are integrated at the HAP so that it can broadcast wireless energy to devices and execute computational tasks, while each device has a rechargeable battery and an EH circuit component which can store the harvested energy to power its operation. The HAP and all the devices are equipped with a single-antenna[2] and the IRS has N reflecting elements. To ease their practical implementation, all the devices and the HAP operate over the same frequency band. The DL WPT and UL offloading are assumed to operate in time-division multiplexing manner by following the typical "harvest-and-then offload" protocol of [7], [8], as shown in Fig. 2. Without loss of generality, we assume that each channel coherence block consists of multiple frames and the operation time of each frame is denoted by T. The channels from the HAP to device k, from the HAP to the IRS, and from the IRS to device k are denoted by $h_{d,k} \in \mathbb{C}$, $\mathbf{g} \in \mathbb{C}^{N\times 1}$, and $\mathbf{h}_{r,k}^H \in \mathbb{C}^{1\times N}$, $\forall k \in \{1,\dots K\}$, respectively. It is worth noting that all the theoretical performance comparisons and the proposed algorithms in this paper are applicable to any wireless channel model. Hence, the type of wireless channel model is not specified here without loss of generality. The channel state information (CSI) is assumed to be perfectly acquired by the HAP, based on the channel acquisition methods discussed in [20]. The results with perfect CSI in this work actually provide a theoretical performance upper bound for the practical system.

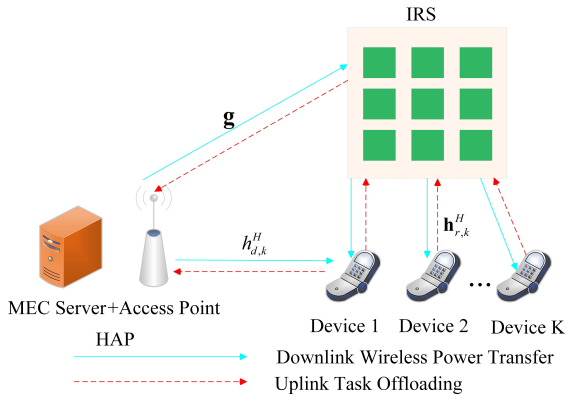

Fig. 1. An IRS-aided wireless powered MEC system.

In this paper, we assume that the partial computation offloading mode is used. Specifically, the computational tasks of each device can be partitioned into two parts: one for local computing and the other for offloading to the HAP. Similar to [7], [8], [10], we assume that the local computing at each device adopts a different component from that used for EH and task offloading. Thus, local computing can be executed throughout the entire frame of duration T. The number of central processor unit (CPU) cycles required for computing one bit of raw data at each device is denoted by C and its value is determined by the properties of the specific application [7]. Let f_k denote the CPU's chosen frequency (cycles-per-second)

[1]Note that the associated problems in this work can be readily extended to the scenario with multiple IRSs as in [35]. As such, our proposed algorithm and analytical results are also applicable to the multiple IRSs case without any modifications.

[2]To unveil the potential benefits of the IRS in WP-MEC systems, we assume that the HAP is equipped with a single antenna. Note that the AO principle harnessed in this paper is also applicable to the case of multiple antennas equipped at the HAP. Specifically, the optimal receive beamformers conceived for the TDMA and NOMA schemes are maximum ratio combiner [14] and minimum mean square error-based arrangements [12], respectively. The BF adopted for DL WPT can be designed as in [14].

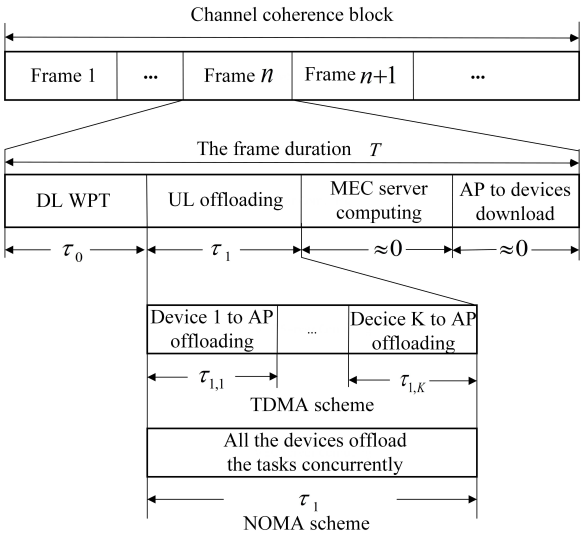

Fig. 2. The structure of a transmission frame.

at device k. Therefore, the bits computed locally by device k and the corresponding dissipated energy by local computing are Tf_k/C and $T\gamma_c f_k^3$, respectively [7]. Note that γ_c represents the computational energy efficiency of specific CPU chip, which depends on the architecture of the chip [5].

As shown in Fig. 2, the transmission frame is comprised of four segments. First, the HAP broadcasts wireless energy to all devices with the aid of the IRS. Then, all the devices can decide to offload their tasks to the HAP by using TDMA or NOMA. In the third stage, the MEC server at the HAP executes the computational tasks offloaded from all devices. Finally, the computational results are downloaded from the HAP to each device. Given the availability of sufficient CPU computing capability at the MEC server, the computation time required by the MEC server may be deemed negligible [7], [8]. Furthermore, since the HAP tends to have a high transmit power and because the computation results are usually of small size, the downloading time may also be neglected [14]. The first and second segments are described as follows.

For DL WPT, an energy signal is broadcasted by the HAP at a constant transmit power P_E for a time duration of τ_0. The reflection phase-shift matrix of the IRS for DL WPT is denoted by $\mathbf{\Theta}_0 = \mathrm{diag}\left(e^{j\theta_1}, \ldots, e^{j\theta_N}\right)$, where $\theta_n \in [0, 2\pi), \forall n$. Since the noise power is much lower than the power received from the HAP [42], we assume that the energy harvested from noise is negligible. Based on the linear EH model[3] of [6]–[8], the energy harvested at device k is

$$E_k = \eta\tau_0 P_E \left|h_{d,k} + \mathbf{h}_{r,k}^H \mathbf{\Theta}_0 \mathbf{g}\right|^2 = \eta\tau_0 P_E \left|h_{d,k} + \mathbf{q}_k^H \mathbf{v}_0\right|^2, \ \forall k, \tag{1}$$

where $\eta \in (0, 1]$ represents the energy conversion efficiency of each device, $\mathbf{q}_k^H = \mathbf{h}_{r,k}^H \mathrm{diag}\left(\mathbf{g}\right)$ and $\mathbf{v}_0 = \left[e^{j\theta_1}, \ldots, e^{j\theta_N}\right]^T$ denotes the IRS BF vector of the DL WPT.

[3]Although the non-linear EH model can capture the relationship between the harvested RF power and the converted direct current power more precisely [15], the key results regarding to theoretical performance comparison between NOMA and TDMA for UL offloading are directly applicable to a more general non-linear EH model. It will be discussed later in Remark 3. The linear EH model is adopted here to facilitate us to explicitly demonstrate the impact of IRS on UL offloading activation condition.

At the UL offloading stage, all devices can offload their tasks to the HAP by the TDMA or NOMA schemes. Adopting different IRS BF vectors during the NOMA/TDMA frame, i.e., DIBF, is in principle possible and may potentially improve the computation rate at the cost of additional signaling overhead. This is because the algorithm is usually executed by the HAP due to the limited processing capability of the IRS and thus the HAP has to feed back the IRS BF vectors to the IRS for reconfiguration. Specifically, we propose three different levels of DIBF schemes as follows: **Case 1**: The same IRS BF vector is adopted during the entire frame; **Case 2**: The IRS BF vectors of the DL WPT and UL offloading can be different, but the same IRS BF vector is adopted in the UL offloading stage for all devices; **Case 3**: The IRS BF vectors of the DL WPT and UL offloading of each device can be different, i.e., K different IRS BF vectors can be used for UL offloading. Considering the aforementioned three cases, the details of UL offloading using TDMA and NOMA are presented as follows.

1) Offloading Using TDMA: The time duration of offloading, namely τ_1, is further partitioned into K orthogonal time slots (TSs). The time duration for the k-th TS is denoted by $\tau_{1,k}, \forall k \in \{1, \ldots K\}$ and $\sum_{k=1}^K \tau_{1,k} = \tau_1$. Device k offloads its data in its k-th TS $\tau_{1,k}$. Let p_k denote the transmit power of device k. For **Case 1**, the DL WPT stage and the UL offloading stage share the same IRS BF vector $\mathbf{v}_0$. In this case, the achievable offloading sum-rate is written as

$$R_{\mathrm{off-case1}}^{\mathrm{TDMA}} = B\sum_{k=1}^{K} \tau_{1,k} \log_2\left(1 + \frac{p_k\left|h_{d,k} + \mathbf{q}_k^H \mathbf{v}_0\right|^2}{\sigma^2}\right), \tag{2}$$

where B represents the system bandwidth and σ^2 denotes the power of the additive white Gaussian noise at the HAP.

For **Case 2**, we adopt $\mathbf{v}_1 = \left[e^{j\varphi_{1,1}}, \ldots, e^{j\varphi_{1,N}}\right]^T$ to denote the common IRS BF vector in the UL offloading stage. The achievable offloading sum-rate is represented as

$$R_{\mathrm{off-case2}}^{\mathrm{TDMA}} = B\sum_{k=1}^{K} \tau_{1,k} \log_2\left(1 + \frac{p_k\left|h_{d,k} + \mathbf{q}_k^H \mathbf{v}_1\right|^2}{\sigma^2}\right). \tag{3}$$

For **Case 3**, the IRS BF vector used for UL offloading in k-th TS is denoted by $\mathbf{v}_{1,k} = \left[e^{j\varphi_{k,1}}, \ldots, e^{j\varphi_{k,N}}\right]^T$. Thus, the achievable offloading sum-rate is given by

$$R_{\mathrm{off-case3}}^{\mathrm{TDMA}} = B\sum_{k=1}^{K} \tau_{1,k} \log_2\left(1 + \frac{p_k\left|h_{d,k} + \mathbf{q}_k^H \mathbf{v}_{1,k}\right|^2}{\sigma^2}\right). \tag{4}$$

2) Offloading Using NOMA: When NOMA is adopted for UL offloading, all the devices simultaneously transmit their respective data to the HAP throughout the whole time duration of τ_1 at the transmit power p_k. To mitigate the inter-user interference, successive interference cancellation (SIC) is performed at the HAP. Taking device k as an example, the HAP will first decode the message of device i, $\forall i < k$, before decoding the message of device k. Then, the offloading message of device i, $\forall i < k$, will be subtracted from the received composite signal. Meanwhile, the offloading message received from device i, $\forall i > k$, is treated as noise. For **Case 1**, the IRS BF vector is denoted by $\mathbf{v}_0$ for the UL offloading stage using NOMA. As

such, the offloading rate of device k is

$$r_k = B\tau_1 \log_2\left(1+\frac{p_k\left|h_{d,k}+\mathbf{q}_k^H\mathbf{v}_0\right|^2}{\sum_{i=k+1}^{K} p_i\left|h_{d,k}+\mathbf{q}_k^H\mathbf{v}_0\right|^2+\sigma^2}\right),\ \forall k. \tag{5}$$

Based on (5), the achievable offloading sum-rate for all the devices can be written as [38]

$$R_{\mathrm{off-case1}}^{\mathrm{NOMA}} = B\tau_1 \log_2\left(1+\frac{\sum_{k=1}^{K} p_k\left|h_{d,k}+\mathbf{q}_k^H\mathbf{v}_0\right|^2}{\sigma^2}\right). \tag{6}$$

Accordingly, the achievable offloading sum-rate of **Case 2** for the NOMA-based UL offloading can be written as

$$R_{\mathrm{off-case2}}^{\mathrm{NOMA}} = B\tau_1 \log_2\left(1+\frac{\sum_{k=1}^{K} p_k\left|h_{d,k}+\mathbf{q}_k^H\mathbf{v}_1\right|^2}{\sigma^2}\right). \tag{7}$$

To ensure a fair comparison for the TDMA and NOMA-based offloading schemes, the number of IRS BF vectors should be set identical for both TDMA and NOMA schemes. As such, **Case 3** is also considered for applying to the NOMA-based offloading. We assume that K IRS BF vectors are available for assisting UL offloading, which are denoted by $\mathbf{v}_{1,i}, \forall i \in \{1,\dots K\}$. Correspondingly, the offloading time τ_1 is partitioned into K TSs and the time duration for the i-th TS is denoted by $\tau_{1,i}, \forall i \in \{1,\dots K\}$ such that $\tau_1 = \sum_{i=1}^{K} \tau_{1,i}$. In the i-th TS, the IRS BF vector $\mathbf{v}_{1,i}$ is employed and all devices transmit simultaneously with power p_k. As such, the corresponding number of offloading bits for all devices in the i-th TS is given by

$$R_{i-\mathrm{case3}}^{\mathrm{NOMA}} = B\tau_{1,i}\log_2\left(1+\frac{\sum_{k=1}^{K} p_k\left|h_{d,k}^H+\mathbf{q}_k^H\mathbf{v}_{1,i}\right|^2}{\sigma^2}\right),\quad \forall i \in \{1,\dots K\}. \tag{8}$$

Then, the total number of offloading bits during the UL offloading stage can be expressed as

$$R_{\mathrm{off-case3}}^{\mathrm{NOMA}} = B\sum_{i=1}^{K}\tau_{1,i}\log_2\left(1+\frac{\sum_{k=1}^{K} p_k\left|h_{d,k}^H+\mathbf{q}_k^H\mathbf{v}_{1,i}\right|^2}{\sigma^2}\right). \tag{9}$$

Due to the limited computing capability of the low-cost IRS and devices, the HAP is in charge of all the algorithmic computations. Then, the HAP sends the optimized IRS BF vectors and resource allocation results to the IRS controller and devices, respectively. It is reasonable to assume that the algorithmic computations can be successfully carried out by the HAP thanks to its powerful computational capability, e.g., [5]–[9], [36]–[38]. Our considered three cases strike a balance between the degrees-of-freedom to adjust the IRS BF vectors and the associated signaling overhead. According to the number of IRS BF vectors available to be employed, the feedback IRS phase shifts information required for **Case 1**, **Case 2**, and **Case 3** are given by N, $2N$, and $(K+1)N$, respectively. Although **Case 3** enjoys the highest flexibility for IRS reconfiguration, its associated signaling overhead is significantly higher than that of **Case 1** and **Case 2**. For the scenarios where the capacity of the feedback link is limited, **Case 1** and **Case 2** may be more appealing than **Case 3** since they require less feedback resources.

B. Problem Formulation

In this paper, we aim for maximizing the total number of computed bits of our IRS-aided WP-MEC systems, by jointly optimizing the IRS BF vectors, the time allocation of WPT and offloading, the transmit power of each device, and the local CPU frequency at each device. Both TDMA and NOMA are considered for UL offloading leading to the following formulation:

1) TDMA-based Offloading: When the TDMA scheme is applied, **Case 1**, **Case 2**, and **Case 3** are considered for evaluating the impact of DIBF on the computation rate. The computation rate maximization problem of **Case 1** can be formulated as[4]

$$\left(\mathrm{P}_{\mathrm{TDMA}}^{\mathrm{case1}}\right): \max_{\tau_0,\tau_{1,k},p_k,\mathbf{v}_0,f_k} R_{\mathrm{off-case1}}^{\mathrm{TDMA}} + \sum\nolimits_{k=1}^{K}\frac{Tf_k}{C} \tag{10a}$$

$$\text{s.t.}\quad \tau_{1,k}p_k + T\gamma_c f_k^3 \le E_k,\ \forall k, \tag{10b}$$

$$\tau_0 + \sum_{k=1}^{K}\tau_{1,k} \le T, \tag{10c}$$

$$\tau_0 \ge 0, \tau_{1,k} \ge 0, p_k \ge 0, f_k \ge 0, \forall k, \tag{10d}$$

$$\left|[\mathbf{v}_0]_n\right| = 1, n = 1,\dots N. \tag{10e}$$

In $\left(\mathrm{P}_{\mathrm{TDMA}}^{\mathrm{case1}}\right)$, (10b) represents the energy harvesting causality constraint that the total dissipated energy cannot be higher than the total harvested energy[5] [7], [8], [14]. Furthermore, (10c) is the constraint on the time duration of the DL WPT and UL offloading, while (10d) contains the non-negativity constraints for the optimization variables and (10e) is the unit-modulus constraint for the IRS BF vector. It is worth noting that for general wirelessly powered communication systems, including WPCN and WP-MEC, the main bottleneck of them is the low amount of energy available for communication, rather than the peak power constraint, e.g., [5]–[9], [36]–[38]. This is because the amount of energy harvested by the devices is generally of a low level due to the severe path loss during WPT and owing to the low energy conversion efficiency. Hence, the peak power constraint is not considered similar to previous works, e.g., [5]–[9], [36]–[38]. For **Case 2** and **Case 3**, the corresponding computation rate maximization problems can be formulated, respectively, as:

$$\left(\mathrm{P}_{\mathrm{TDMA}}^{\mathrm{case2}}\right): \max_{\tau_0,\tau_{1,k},p_k,\mathbf{v}_0,\mathbf{v}_1,f_k} R_{\mathrm{off-case2}}^{\mathrm{TDMA}} + \sum\nolimits_{k=1}^{K}\frac{Tf_k}{C} \tag{11a}$$

$$\text{s.t.}\quad \left|[\mathbf{v}_1]_n\right| = 1, n = 1,\dots N, \tag{11b}$$

$$(10\text{b}), (10\text{c}), (10\text{d}), (10\text{e}), \tag{11c}$$

[4]To facilitate comparing the fundamental limits of the achievable computation rate for both the TDMA and NOMA-based offloading schemes, the quality of service (QoS) constraints of the individual devices are not considered here. Nonetheless, the proposed algorithm is potentially applicable to the operating scenarios under specific QoS constraints. Please refer to Remark 5 in Section V for further details.

[5]Since we assume that each channel coherence block is long enough to accommodate multiple frames, the energy consumed here is comprised of two parts. Explicitly, part of it is used for UL offloading in the current frame, while the remaining part is assigned to local computing throughout the UL offloading process during the current frame and during the DL WPT in the next frame. Note that constraint (10b) was also adopted in [7], [8], [14].

$$(\mathrm{P}^{\mathrm{case3}}_{\mathrm{TDMA}}): \max_{\tau_0,\tau_{1,k},p_k,\mathbf{v}_0,\mathbf{v}_{1,k},f_k} R^{\mathrm{TDMA}}_{\mathrm{off-case3}}+\sum\nolimits_{k=1}^{K}\frac{Tf_k}{C} \quad (12a)$$

$$\text{s.t.} \quad \left|[\mathbf{v}_{1,k}]_n\right|=1, \forall n, \ \ \forall k, \quad (12b)$$

$$(10b), (10c), (10d), (10e). \quad (12c)$$

2) NOMA-based Offloading: When NOMA is applied for UL offloading, the corresponding computation rate maximization problems are formulated according to the aforementioned three cases, respectively, as follows:

$$(\mathrm{P}^{\mathrm{case1}}_{\mathrm{NOMA}}): \max_{\tau_0,\tau_1,p_k,\mathbf{v}_0,f_k} R^{\mathrm{NOMA}}_{\mathrm{off-case1}}+\sum\nolimits_{k=1}^{K}\frac{Tf_k}{C} \quad (13a)$$

$$\text{s.t.} \quad \tau_1 p_k + T\gamma_c f_k^3 \le E_k, \ \ \forall k, \quad (13b)$$

$$\tau_0+\tau_1 \le T, \quad (13c)$$

$$\tau_0 \ge 0, \tau_1 \ge 0, p_k \ge 0, f_k \ge 0, \forall k, \quad (13d)$$

$$(10e), \quad (13e)$$

$$(\mathrm{P}^{\mathrm{case2}}_{\mathrm{NOMA}}): \max_{\substack{\tau_0,\tau_1,p_k,\\ \mathbf{v}_0,\mathbf{v}_1,f_k}} R^{\mathrm{NOMA}}_{\mathrm{off-case2}}+\sum\nolimits_{k=1}^{K}\frac{Tf_k}{C} \quad (14a)$$

$$\text{s.t.} \quad (10e), (11b), (13b), (13c), (13d), \quad (14b)$$

$$(\mathrm{P}^{\mathrm{case3}}_{\mathrm{NOMA}}): \max_{\substack{\tau_0,\tau_{1,i},p_k,\\ \mathbf{v}_0,\mathbf{v}_{1,i},f_k}} R^{\mathrm{NOMA}}_{\mathrm{off-case3}}+\sum\nolimits_{k=1}^{K}\frac{Tf_k}{C} \quad (15a)$$

$$\text{s.t.} \quad \tau_0+\sum_{i=1}^{K}\tau_{1,i} \le T, \quad (15b)$$

$$\tau_0 \ge 0, \tau_{1,i} \ge 0,$$

$$p_k \ge 0, f_k \ge 0, \forall k, \forall i, \quad (15c)$$

$$\left|[\mathbf{v}_{1,i}]_n\right|=1, n=1,\dots N, \ \ \forall i, \quad (15d)$$

$$(10e), \ (13b). \quad (15e)$$

III. TDMA or NOMA for UL Offloading?

When multiple devices are activated for UL offloading, it still remains unknown which MA scheme is more efficient for UL offloading in terms of computation rate, especially when considering the impact of the IRS. To answer this question, the theoretical performance comparison between NOMA and TDMA-based UL offloading is provided in this section. First, the impact of DIBF on the computation rate of both NOMA and TDMA-based WP-MEC systems is analyzed. Then, we analytically compare the computation rate achieved by NOMA and TDMA schemes for **Cases 1, 2, and 3**.

A. Impact of DIBF on NOMA and TDMA

For notational simplicity, we use $R^{\mathrm{case}-m}_{\mathrm{TDMA}}$ and $R^{\mathrm{case}-m}_{\mathrm{NOMA}}$ to denote the sum computation rate for **Case** $m, (m=1,2,3)$ of TDMA and NOMA at the optimal solution, respectively. To shed light on the impact of DIBF on the computation rate of the NOMA and TDMA schemes, we first introduce the following lemmas.

Lemma 1: For IRS-aided WP-MEC systems employing NOMA for offloading, it follows that $R^{\mathrm{case1}}_{\mathrm{NOMA}} \le R^{\mathrm{case2}}_{\mathrm{NOMA}} = R^{\mathrm{case3}}_{\mathrm{NOMA}}$.

Proof: Assume that an optimal solution of $(\mathrm{P}^{\mathrm{case3}}_{\mathrm{NOMA}})$ is given by $\{\tau_0^*, \tau_{1,i}^*, p_k^*, f_k^*, \mathbf{v}_0^*, \mathbf{v}_{1,i}^*\}$. Then, the optimal value of $(\mathrm{P}^{\mathrm{case3}}_{\mathrm{NOMA}})$ can be expressed as

$$R^{\mathrm{case3}}_{\mathrm{NOMA}} = \sum_{i=1}^{K}\tau_{1,i}^*\log_2\left(1+\frac{\sum_{k=1}^{K}p_k^*\left|h_{d,k}+\mathbf{q}_k^H\mathbf{v}_{1,i}^*\right|^2}{\sigma^2}\right) + \sum_{k=1}^{K}\frac{Tf_k^*}{C}. \quad (16)$$

There always exists an IRS BF vector denoted by $\mathbf{v}_{1,p}^*$, $p \in \{1,\cdots,K\}$, which satisfies $\mathbf{v}_{1,p}^* = \arg\max_{\mathbf{v}_{1,i}^*, i\in\{1,\cdots,K\}} \sum_{k=1}^{K} p_k^*\left|h_{d,k}^H+\mathbf{q}_k^H\mathbf{v}_{1,i}^*\right|^2$. As such, we have

$$\begin{aligned} R^{\mathrm{case3}}_{\mathrm{NOMA}} &\le \sum_{i=1}^{K}\tau_{1,i}^*\log_2\left(1+\frac{\sum_{k=1}^{K}p_k^*\left|h_{d,k}+\mathbf{q}_k^H\mathbf{v}_{1,p}^*\right|^2}{\sigma^2}\right) + \sum_{k=1}^{K}\frac{Tf_k^*}{C} \\ &= \tilde{\tau}_1\log_2\left(1+\frac{\sum_{k=1}^{K}p_k^*\left|h_{d,k}+\mathbf{q}_k^H\mathbf{v}_{1,p}^*\right|^2}{\sigma^2}\right) + \sum_{k=1}^{K}\frac{Tf_k^*}{C} \le R^{\mathrm{case2}}_{\mathrm{NOMA}}, \end{aligned} \quad (17)$$

where $\tilde{\tau}_1 = \sum_{i=1}^{K}\tau_{1,i}^*$. The equality holds if $\mathbf{v}_{1,i}^* = \mathbf{v}_{1,p}^*, \forall i$. Meanwhile, by setting $\mathbf{v}_{1,i} = \mathbf{v}_{1,j}, \forall i,j$, problem $(\mathrm{P}^{\mathrm{case3}}_{\mathrm{NOMA}})$ is reduced to $(\mathrm{P}^{\mathrm{case2}}_{\mathrm{NOMA}})$, which yields $R^{\mathrm{case2}}_{\mathrm{NOMA}} \le R^{\mathrm{case3}}_{\mathrm{NOMA}}$. Thus, we have $R^{\mathrm{case2}}_{\mathrm{NOMA}} = R^{\mathrm{case3}}_{\mathrm{NOMA}}$. Similarly, problem $(\mathrm{P}^{\mathrm{case2}}_{\mathrm{NOMA}})$ is reduced to $(\mathrm{P}^{\mathrm{case1}}_{\mathrm{NOMA}})$ by setting $\mathbf{v}_1 = \mathbf{v}_0$, thus we have $R^{\mathrm{case1}}_{\mathrm{NOMA}} \le R^{\mathrm{case2}}_{\mathrm{NOMA}}$. ∎

Lemma 2: For IRS-aided WP-MEC systems employing TDMA for offloading, it follows that $R^{\mathrm{case1}}_{\mathrm{TDMA}} \le R^{\mathrm{case2}}_{\mathrm{TDMA}} \le R^{\mathrm{case3}}_{\mathrm{TDMA}}$.

Proof: By setting $\mathbf{v}_1 = \mathbf{v}_0$, problem $(\mathrm{P}^{\mathrm{case2}}_{\mathrm{TDMA}})$ is reduced to $(\mathrm{P}^{\mathrm{case1}}_{\mathrm{TDMA}})$, which yields $R^{\mathrm{case1}}_{\mathrm{TDMA}} \le R^{\mathrm{case2}}_{\mathrm{TDMA}}$. For **Case 3**, the equivalent channel power gain of each device can be maximized by setting $\mathbf{v}_{1,k}$ to align the cascaded link with the direct link $h_{d,k}^H$. Thus, $\left|h_{d,k}+\mathbf{q}_k^H\mathbf{v}_{1,k}^*\right|^2 \ge \left|h_{d,k}+\mathbf{q}_k^H\mathbf{v}_1^*\right|^2$ holds for device $k, \forall k$, which yields $R^{\mathrm{case2}}_{\mathrm{TDMA}} \le R^{\mathrm{case3}}_{\mathrm{TDMA}}$. ∎

Lemma 1 and Lemma 2 provide the following insights and also serve as the theoretical foundation for comparing TDMA and NOMA-based offloading, which will be discussed later.

- For NOMA-based UL offloading, varying the IRS BF vectors in the UL offloading stage does not necessarily attain performance improvements over a static IRS BF vector. By contrast, for TDMA-based UL offloading, the computation rate can be further improved by varying IRS BF vectors for UL offloading.
- For both TDMA and NOMA-based WP-MEC systems, having different IRS BF vectors for the DL WPT and UL offloading generally outperforms its counterpart using the same IRS BF vector throughout the entire frame.

B. TDMA versus NOMA-based UL Offloading

To compare the achievable computation rate performance between offloading using TDMA and NOMA, the relationship

between $(\mathrm{P}^{\mathrm{case2}}_{\mathrm{TDMA}})$ and $(\mathrm{P}^{\mathrm{case2}}_{\mathrm{NOMA}})$ is presented in the following theorem.

Theorem 1: Assuming that $\left\{\tau_0^*, \tau_{1,k}^*, p_k^*, \mathbf{v}_0^*, \mathbf{v}_1^*, f_k^*\right\}$ and $\{\tau_0^\star, \tau_1^\star, p_k^\star, \mathbf{v}_0^\star, \mathbf{v}_1^\star, f_k^\star\}$ are the optimal solutions of $(\mathrm{P}^{\mathrm{case2}}_{\mathrm{TDMA}})$ and $(\mathrm{P}^{\mathrm{case2}}_{\mathrm{NOMA}})$, respectively, we have $R^{\mathrm{case2}}_{\mathrm{TDMA}} = R^{\mathrm{case2}}_{\mathrm{NOMA}}$ with $\tau_0^\star = \tau_0^*, \tau_1^\star = \sum_{k=1}^K \tau_{1,k}^*, e_k^\star = e_k^*, \mathbf{v}_0^\star = \mathbf{v}_0^*, \mathbf{v}_1^\star = \mathbf{v}_1^*$ and $f_k^\star = f_k^*$, where $e_k^\star = p_k^\star \tau_1^\star$ and $e_k^* = p_k^* \tau_{1,k}^*$.

Proof: Please see Appendix A. ∎

Note that the similar results presented in Theorem 1 can be directly extended to capture the interrelation between $(\mathrm{P}^{\mathrm{case1}}_{\mathrm{TDMA}})$ and $(\mathrm{P}^{\mathrm{case1}}_{\mathrm{NOMA}})$, i.e., $R^{\mathrm{case1}}_{\mathrm{TDMA}} = R^{\mathrm{case1}}_{\mathrm{NOMA}}$. Theorem 1 explicitly shows that the solutions of problem $(\mathrm{P}^{\mathrm{case1}}_{\mathrm{NOMA}})$ and $(\mathrm{P}^{\mathrm{case2}}_{\mathrm{NOMA}})$ can be directly obtained based on those of $(\mathrm{P}^{\mathrm{case1}}_{\mathrm{TDMA}})$ and $(\mathrm{P}^{\mathrm{case2}}_{\mathrm{TDMA}})$, respectively.

Remark 1: The results presented in Lemma 1, Lemma 2, and Theorem 1 answer the fundamental question regarding the computation rate comparison between offloading using TDMA and NOMA. Specifically, the comparison outcome depends on which DIBF scheme is applied. For **Case 1** and **Case 2**, it is shown that the same computation rate can be achieved by using TDMA and NOMA for offloading. Since the computation rate of TDMA can be further improved by adapting IRS BF vectors over different TSs in the UL offloading stage, the computation rate of TDMA becomes higher than that of NOMA for **Case 3** at the cost of extra signaling overhead. As such, we have the inequality chain as follows:

$$\begin{aligned} R^{\mathrm{case1}}_{\mathrm{TDMA}} &= R^{\mathrm{case1}}_{\mathrm{NOMA}} \le R^{\mathrm{case2}}_{\mathrm{TDMA}} \\ &= R^{\mathrm{case2}}_{\mathrm{NOMA}} = R^{\mathrm{case3}}_{\mathrm{NOMA}} \le R^{\mathrm{case3}}_{\mathrm{TDMA}}. \end{aligned} \tag{18}$$

Remark 2: Considering the high C regime, i.e., $C \to +\infty$, which implies that the device has nearly no computing capability to deal with computationally intensive tasks, the computations completely rely on offloading the tasks to MEC servers. In this case, the computation rate maximization problem is equivalent to the throughput maximization problem of WPCNs. For **Case 2**, our previous work [38] unveiled that the same IRS BF vector can be exploited for the DL and UL in WPCNs without loss of optimality, i.e., $\mathbf{v}_0^* = \mathbf{v}_1^*$. Based on the results provided in Theorem 1, we have the following relationship in the high C regime:

$$\begin{aligned} R^{\mathrm{case1}}_{\mathrm{TDMA}} &= R^{\mathrm{case1}}_{\mathrm{NOMA}} = R^{\mathrm{case2}}_{\mathrm{TDMA}} \\ &= R^{\mathrm{case2}}_{\mathrm{NOMA}} = R^{\mathrm{case3}}_{\mathrm{NOMA}} \le R^{\mathrm{case3}}_{\mathrm{TDMA}}. \end{aligned} \tag{19}$$

In contrast to (18), (19) suggests that for **Case 2**, DL WPT and UL offloading can adopt the same IRS BF vector without loss of optimality at a lower signaling overhead.

Remark 3: Note that the theoretical comparison provided in Remark 2 can be directly extended to a more general non-linear EH model. For a general EH model, the output direct current power can be generally expressed as a function of the input RF power, i.e, $Q_k\left(P_E\left|h_{d,k}^H + \mathbf{q}_k^H \mathbf{v}_0^*\right|^2\right)$. Replacing $\eta P_E\left|h_{d,k} + \mathbf{q}_k^H \mathbf{v}_0^*\right|^2$ by $Q_k\left(P_E\left|h_{d,k} + \mathbf{q}_k^H \mathbf{v}_0^*\right|^2\right)$ in Appendix A, the results can be directly obtained through similar steps.

Remark 4: It can be readily verified the conclusions regarding TDMA versus NOMA drawn in terms of computation rate are also applicable to IRS-aided WP-MEC systems employing binary offloading.

IV. UL Offloading activation Condition in single-user Systems

Before deriving the solutions of the aforementioned computation rate maximization problems, we consider the special case of a single-user setup, i.e., $K = 1$, to gain important insights into the efficiency of IRSs for UL offloading activation. Note that the conclusions drawn in this section regarding the effectiveness of the IRS for activating UL offloading are also valid for general multi-user systems, which will be verified by simulations in Section VI. In the single-user case, the MA schemes have no impact on the results, and thus the computation rate maximization problems are simplified to:

$$\max_{\tau_0,\tau_1,p,\mathbf{v},f} \quad B\tau_1 \log_2\left(1 + \frac{p\left|h_d + \mathbf{q}^H\mathbf{v}\right|^2}{\sigma^2}\right) + \frac{Tf}{C} \tag{20a}$$

$$\text{s.t.} \quad \tau_1 p + T\gamma_c f^3 \le \tau_0 \eta P_E \left|h_d + \mathbf{q}^H\mathbf{v}\right|^2, \tag{20b}$$

$$\tau_0 + \tau_1 \le T, \tag{20c}$$

$$\tau_0 \ge 0, \tau_1 \ge 0, p \ge 0, f \ge 0, \tag{20d}$$

$$\left|[\mathbf{v}]_n\right| = 1, n = 1, \ldots N. \tag{20e}$$

Problem (20) has not been investigated in previous articles to the best of our knowledge, e.g., [40], [41]. Note that for a WP-MEC system, UL offloading may not be activated, when suffering from severe wireless channel conditions. Hence, we focus our attention on a single-user case to unveil the impact of IRSs on the UL offloading activation condition. For problem (20), the optimal IRS BF vector $\mathbf{v}$ can be directly obtained as $[\mathbf{v}^*]_n = e^{j\left(\left(\arg\left(h_d^H\right) + \arg\left([\mathbf{q}]_n\right)\right)\right)}$, which aligns the cascaded channel between a typical device and the HAP via the IRS with the end-to-end channel. By setting $\mathbf{v}$ as the optimal form, the channel power gain between a typical device and HAP is determined. Let $h = \left|h_d^H + \mathbf{q}^H\mathbf{v}^*\right|^2$ for notational simplicity. Then, problem (20) can be further transformed into a resource allocation optimization problem (OP) as follows

$$\max_{\tau_0,\tau_1,e,f} \quad B\tau_1 \log_2\left(1 + \frac{eh^2}{\tau_1\sigma^2}\right) + \frac{Tf}{C} \tag{21a}$$

$$\text{s.t.} \quad e + T\gamma_c f^3 \le \tau_0 \eta P_E h, \tag{21b}$$

$$\tau_0 \ge 0, \tau_1 \ge 0, e \ge 0, f \ge 0, \tag{21c}$$

$$\text{(20c)}, \tag{21d}$$

where $e = \tau_1 p$. It may be readily shown that problem (21) is a convex OP. By analyzing the KKT conditions of problem (21), the UL offloading activation condition admitting a threshold-based structure and the optimal solution of problem (21) are obtained in the following proposition.

Proposition 1: For the single-user setup, UL offloading for the typical device will be activated if and only if the following condition is satisfied,

$$P_E > \mathrm{thre}\,(h) = \gamma_c \frac{1}{\eta h}\left(\frac{\left(\sigma^2 + p^* h\right)\ln 2}{3Ch\gamma_c B}\right)^{\frac{3}{2}}, \tag{22}$$

where p^* is the unique solution of

$$\begin{aligned} G\,(p,h) \triangleq \log_2\left(1 + \frac{ph}{\sigma^2}\right) - \frac{ph}{(\sigma^2 + ph)\ln 2} \\ - \eta P_E \frac{h^2}{(\sigma^2 + ph)\ln 2} = 0. \end{aligned} \tag{23}$$

In this case, the optimal solution for problem (20), denoted by $\{\tau_0^*, \tau_1^*, f^*, e^*\}$, is given by

$$f^* = \sqrt{\frac{(\sigma^2 + p^* h)\ln 2}{3Ch\gamma_c B}}, \tau_1^* = \frac{\eta P_E h - \gamma_c \left(\frac{\left(\sigma^2 + p^* h\right)\ln 2}{3Ch\gamma_c B}\right)^{\frac{3}{2}}}{p^* + \eta P_E h} T,$$
$$\tau_0^* = T - \tau_1^*, e^* = \tau_1^* p^*. \tag{24}$$

In contrast, if (30) is not satisfied, the UL offloading is not activated and the corresponding optimal solution is given by

$$\tau_0^* = T, \tau_1^* = 0, f^* = \left(\frac{P_E \eta h}{\gamma_c}\right)^{1/3}, e^* = 0. \tag{25}$$

Proof: Please see Appendix B. ∎

Proposition 1 directly provides the optimal solution of problem (20) in a (semi) closed-form, which thus avoids the computational complexity incurred by using numerical optimization solvers, such as CVX. Moreover, Proposition 1 unveils the UL offloading activation condition from a mathematical perspective. Specifically, it shows that a typical device would prefer UL offloading for maximizing its computation rate, when the transmit power of the HAP is higher than a minimum threshold $\mathrm{thre}(h)$, which depends on the channel's power gain h.

Proposition 2: The threshold $\mathrm{thre}(h)$ decreases with the equivalent channel power gain h.

Proof: Since $\ln(\mathrm{thre}(h))$ has the same monotonic relationship with h as that of $\mathrm{thre}(h)$, we focus our attention on showing that $\ln(\mathrm{thre}(h))$ decreases with h instead. Taking the first order derivative of $\ln(\mathrm{thre}(h))$ with respect to h, we obtain

$$\frac{\partial \ln(\mathrm{thre}(h))}{\partial h} = \frac{\partial\left(-\frac{5}{2}\ln h + \frac{3}{2}\ln\left(\sigma^2 + hp^*(h)\right)\right)}{\partial h}$$
$$= -\frac{5}{2}\frac{1}{h} + \frac{3}{2}\frac{\bar{p} + h\frac{dp^*(h)}{dh}}{\sigma^2 + hp^*(h)}. \tag{26}$$

Note that p^* is a function of h, which is determined by (23). As such, we use $p^*(h)$ instead of p^* in the following. Based on the method of implicit differentiation, we obtain

$$\frac{\partial p^*(h)}{\partial h} = -\frac{\partial G(p,h)/\partial h}{\partial G(p,h)/\partial p} = \frac{\eta P_E\left(2\sigma^2 + hp^*(h)\right) - \left(p^*(h)\right)^2}{h\left(\eta P_E h + p^*(h)\right)}. \tag{27}$$

Substituting (27) into (26) yields

$$\frac{\partial \ln(\mathrm{thre}(h))}{\partial h} = \frac{-\frac{5}{2}p^*(h) - \frac{1}{2}\eta P_E h}{h\left(p^*(h) + \eta P_E h\right)} < 0. \tag{28}$$

Thus, $\mathrm{thre}(h)$ decreases with h. ∎

Proposition 1 and Proposition 2 serve as a solid theoretical foundation for further investigating the impact of IRSs on the UL offloading activation condition. For ease of exposition, we assume that the IRS can establish pure line-of-sight (LoS) links with both the device and the AP. By setting the IRS BF vector as the optimal form, the equivalent channel power gain can be formulated as

$$h = \left|h_d + \mathbf{q}^H \mathbf{v}^*\right|^2$$
$$= \beta d_{\mathrm{AD}}^{-\alpha_{\mathrm{AD}}}\left(1 + N\sqrt{d_{\mathrm{AD}}^{\alpha_{\mathrm{AD}}} d_{\mathrm{AI}}^{-\alpha_{\mathrm{AI}}}}\sqrt{\beta d_{\mathrm{ID}}^{-\alpha_{\mathrm{ID}}}}\right)^2, \tag{29}$$

where d_{AD} (α_{AD}), d_{AI} (α_{AI}), and d_{ID} (α_{ID}) denote the length (path-loss exponent) of the HAP-device, HAP-IRS, and IRS-device links, respectively, and β represents the channel power gain at a reference distance of 1 meter (m).

Remark 5: For a specific dominant LoS scenario, the UL offloading activation condition can be expressed as

$$P_E > \frac{\gamma_c}{\eta\beta d_{\mathrm{AD}}^{-\alpha_{\mathrm{AD}}}}$$
$$\times \left(\frac{\left(\sigma^2 + p^*\left(1 + N\sqrt{\beta d_{\mathrm{ID}}^{-\alpha_{\mathrm{ID}}} d_{\mathrm{AD}}^{\alpha_{\mathrm{AD}}} d_{\mathrm{AI}}^{-\alpha_{\mathrm{AI}}}}\right)^2\right)\ln 2}{3C\left(1 + N\sqrt{\beta d_{\mathrm{ID}}^{-\alpha_{\mathrm{ID}}} d_{\mathrm{AD}}^{\alpha_{\mathrm{AD}}} d_{\mathrm{AI}}^{-\alpha_{\mathrm{AI}}}}\right)^{\frac{10}{3}}\gamma_c B}\right)^{\frac{3}{2}}. \tag{30}$$

It is plausible that the value of h using IRSs becomes $\left(1 + N\sqrt{\beta d_{\mathrm{ID}}^{-\alpha_{\mathrm{ID}}} d_{\mathrm{AD}}^{\alpha_{\mathrm{AD}}} d_{\mathrm{AI}}^{-\alpha_{\mathrm{AI}}}}\right)^2$ times higher than that without IRSs. By increasing the number of IRS elements N, the channel power gain h can be significantly increased, which substantially reduces the threshold $\mathrm{thre}(h)$ for UL offloading. Thus, a typical device is more willing to perform task offloading upon increasing of N due to the improved channel conditions. This confirms the practicality of deploying IRSs in next generation communication networks.

V. Proposed Solutions for General Multi-user Systems

In this section, we focus our attention on solving the computation rate maximization problems of TDMA-based UL offloading, i.e., $\left(\mathrm{P}_{\mathrm{TDMA}}^{\mathrm{case1}}\right)$, $\left(\mathrm{P}_{\mathrm{TDMA}}^{\mathrm{case2}}\right)$, and $\left(\mathrm{P}_{\mathrm{TDMA}}^{\mathrm{case3}}\right)$. Solving the same problems for NOMA is similar to those of TDMA according to the results of Section III.

A. AO Algorithm Proposed for Solving $\left(\mathrm{P}_{\mathrm{TDMA}}^{\mathrm{case1}}\right)$ and $\left(\mathrm{P}_{\mathrm{TDMA}}^{\mathrm{case2}}\right)$

Since problem $\left(\mathrm{P}_{\mathrm{TDMA}}^{\mathrm{case2}}\right)$ is more complex than $\left(\mathrm{P}_{\mathrm{TDMA}}^{\mathrm{case1}}\right)$, we commence with **Case 2**, i.e., $\left(\mathrm{P}_{\mathrm{TDMA}}^{\mathrm{case2}}\right)$. It will be shown later in this section that an algorithm designed for solving $\left(\mathrm{P}_{\mathrm{TDMA}}^{\mathrm{case2}}\right)$ may also be directly applicable to $\left(\mathrm{P}_{\mathrm{TDMA}}^{\mathrm{case1}}\right)$. For problem $\left(\mathrm{P}_{\mathrm{TDMA}}^{\mathrm{case2}}\right)$, the optimization variable p_k is closely coupled with the variables $\tau_{1,k}$ and $\mathbf{v}_1$, while τ_0 is coupled with $\mathbf{v}_0$. Moreover, the unit-modulus constraints in (10e) and (11b) render problem $\left(\mathrm{P}_{\mathrm{TDMA}}^{\mathrm{case2}}\right)$ non-convex. In order to deal with the closely-coupled non-convex terms in problem $\left(\mathrm{P}_{\mathrm{TDMA}}^{\mathrm{case2}}\right)$, we decompose the original problem into a pair of subproblems. Specifically, the resource allocation OP with respect to $\{\tau_0, \tau_{1,k}, p_k, f_k\}$ and the IRS BF OP with respect to $\{\mathbf{v}_0, \mathbf{v}_1\}$ can be efficiently solved in an alternating manner as described next.

1) Resource Allocation Optimization: Under any given feasible IRS BF vectors $\mathbf{v}_0$ and $\mathbf{v}_1$, the resource allocation OP with respect to $\{\tau_0, \tau_{1,k}, p_k, f_k\}$ may be written as

$$\max_{\tau_0, \tau_{1,k}, p_k, f_k} \quad B\sum_{k=1}^{K}\tau_{1,k}\log_2\left(1 + \frac{p_k g_k^{\mathrm{off}}}{\sigma^2}\right) + \sum_{k=1}^{K}\frac{T f_k}{C} \tag{31a}$$
$$\text{s.t.} \quad \tau_{1,k} p_k + T\gamma_c f_k^3 \le \tau_0 \eta P_E h_k^{\mathrm{wpt}} \ \ \forall k, \tag{31b}$$
$$(10\mathrm{c}),\ (10\mathrm{d}). \tag{31c}$$

Here, we use $h_k^{\mathrm{wpt}} = \left|h_{d,k} + \mathbf{q}_k^H \mathbf{v}_0\right|^2$ and $g_k^{\mathrm{off}} = \left|h_{d,k} + \mathbf{q}_k^H \mathbf{v}_1\right|^2$ to denote the equivalent channel power gains of

device k for the DL WPT and UL offloading links, respectively. Observe that (31) is still a non-convex OP due the coupled variables $\tau_{1,k}$, p_k in (31b) and the non-concave objective function. To tackle this issue, problem (31) can be equivalently transformed into the following OP by letting $e_k = \tau_{1,k} p_k$

$$\max_{\tau_0,\tau_{1,k},e_k,f_k} \; B\sum_{k=1}^{K}\tau_{1,k}\log_2\left(1+\frac{e_k g_k^{\rm off}}{\tau_{1,k}\sigma^2}\right)+\sum_{k=1}^{K}\frac{Tf_k}{C} \quad (32a)$$

$$\text{s.t.} \quad e_k + T\gamma_c f_k^3 \le \tau_0 \eta P_E h_k^{\rm wpt} \;\; \forall k, \quad (32b)$$

$$\tau_0 \ge 0, \tau_{1,k} \ge 0, e_k \ge 0, f_k \ge 0 \;\; \forall k, \quad (32c)$$

$$(10c). \quad (32d)$$

It can be verified that problem (32) is a convex OP whose optimal solutions can be efficiently obtained by standard numerical methods, e.g., the interior point method [43].

2) Optimization of IRS BF Vectors: For any given feasible set $\{\tau_0, \tau_{1,k}, p_k, f_k\}$, the OP with respect to $\{\mathbf{v}_0, \mathbf{v}_1\}$ can be written as

$$\max_{\mathbf{v}_0,\mathbf{v}_1} B\sum_{k=1}^{K}\tau_{1,k}\log_2\left(1+\frac{p_k\left|h_{d,k}+\mathbf{q}_k^H\mathbf{v}_1\right|^2}{\sigma^2}\right)+\sum_{k=1}^{K}\frac{Tf_k}{C} \quad (33a)$$

$$\text{s.t.} \quad (10b),\ (10e),\ (11b). \quad (33b)$$

Although $\mathbf{v}_0$ does not appear in objective function (33a) directly, it appears in constraint (10b) and determines the total harvested energy at each device, which has direct impacts on optimizing the transmit power and local computing frequency for each device when solving problem (32) in the next iteration. As such, $\mathbf{v}_1$ and $\mathbf{v}_0$ need to be jointly optimized for achieving the higher objective value. Problem (33) is challenging to solve due to the non-concave objective function and non-convex constraints in (33b). To make problem (33) more tractable, we first relax the unit-modulus constraints (10e) and (11b) into $|[\mathbf{v}_0]_n| \le 1$ and $|[\mathbf{v}_1]_n| \le 1$, which yields the following problem:

$$\max_{\mathbf{v}_0,\mathbf{v}_1} \; B\sum_{k=1}^{K}\tau_{1,k}\log_2\left(1+\frac{p_k\left|h_{d,k}+\mathbf{q}_k^H\mathbf{v}_1\right|^2}{\sigma^2}\right)+\sum_{k=1}^{K}\frac{Tf_k}{C} \quad (34a)$$

$$\text{s.t.} \quad |[\mathbf{v}_0]_n| \le 1, n = 1, \;\ldots N, \quad (34b)$$

$$|[\mathbf{v}_1]_n| \le 1, n = 1, \;\ldots N, \quad (34c)$$

$$(10b). \quad (34d)$$

In the following, we focus our attention on the IRS BF vector OP relying on continuous amplitudes. To handle the non-concave objective function, we introduce a slack variable S_k and reformulate problem (34) as follows

$$\max_{S_k,\mathbf{v}_0,\mathbf{v}_1} \; B\sum_{k=1}^{K}\tau_{1,k}\log_2\left(1+\frac{p_k S_k}{\sigma^2}\right)+\sum_{k=1}^{K}\frac{Tf_k}{C} \quad (35a)$$

$$\text{s.t.} \quad (10b),\ (34b),\ (34c), \quad (35b)$$

$$S_k \le \left|h_{d,k}+\mathbf{q}_k^H\mathbf{v}_1\right|^2, \;\; \forall k. \quad (35c)$$

Note that problem (35) is equivalent to problem (34) since constraint (35c) is satisfied with equality at the optimal solution. Problem (35) is still a non-convex OP due to constraints (35b) and (35c). However, the convexity of $\left|h_{d,k}+\mathbf{q}_k^H\mathbf{v}_0\right|^2$ and $\left|h_{d,k}+\mathbf{q}_k^H\mathbf{v}_1\right|^2$ allows us to apply the SCA technique to deal with constraints (10b) and (35c). Let $\left|h_{d,k}+\mathbf{q}_k^H\mathbf{v}_0\right|^2 = \left|\bar{\mathbf{q}}_k^H\bar{\mathbf{v}}_0\right|^2$ and $\left|h_{d,k}+\mathbf{q}_k^H\mathbf{v}_1\right|^2 = \left|\bar{\mathbf{q}}_k^H\bar{\mathbf{v}}_1\right|^2$, where $\bar{\mathbf{v}}_0 = \left[\bar{\mathbf{v}}_0^H, 1\right]^H$, $\bar{\mathbf{v}}_1 = \left[\bar{\mathbf{v}}_1^H, 1\right]^H$, and $\bar{\mathbf{q}}_k^H = \left[\mathbf{q}_k^H, h_{d,k}\right]$. Specifically, we use l ($l \in \mathbb{Z}^+$) to denote the iteration index. At the l-th iteration, where a given local point is denoted by $\left\{\bar{\mathbf{v}}_0^{(l)}, \bar{\mathbf{v}}_1^{(l)}\right\}$, we have

$$\begin{aligned}\left|h_{d,k}+\mathbf{q}_k^H\mathbf{v}_0\right|^2 &= \bar{\mathbf{v}}_0^H\mathbf{Q}_k\bar{\mathbf{v}}_0 \\ &\ge 2\mathrm{Re}\left(\bar{\mathbf{v}}_0^{(l)H}\mathbf{Q}_k\bar{\mathbf{v}}_0\right)-\bar{\mathbf{v}}_0^{(l)H}\mathbf{Q}_k\bar{\mathbf{v}}_0^{(l)}, \quad (36)\end{aligned}$$

$$\begin{aligned}\left|h_{d,k}+\mathbf{q}_k^H\mathbf{v}_1\right|^2 &= \bar{\mathbf{v}}_1^H\mathbf{Q}_k\bar{\mathbf{v}}_1 \\ &\ge 2\mathrm{Re}\left(\bar{\mathbf{v}}_1^{(l)H}\mathbf{Q}_k\bar{\mathbf{v}}_1\right)-\bar{\mathbf{v}}_1^{(l)H}\mathbf{Q}_k\bar{\mathbf{v}}_1^{(l)}, \quad (37)\end{aligned}$$

where $\mathbf{Q}_k = \bar{\mathbf{q}}_k\bar{\mathbf{q}}_k^H$. As such, problem (35) can be transformed into the following tractable form

$$\max_{S_k,\mathbf{v}_0,\mathbf{v}_1} \; B\sum_{k=1}^{K}\tau_{1,k}\log_2\left(1+\frac{p_k S_k}{\sigma^2}\right)+\sum_{k=1}^{K}\frac{Tf_k}{C} \quad (38a)$$

$$\text{s.t.} \quad \tau_{1,k}p_k + T\gamma_c f_k^3 \le \eta P_E\tau_0\left(2\mathrm{Re}\left(\bar{\mathbf{v}}_0^{(l)H}\mathbf{Q}_k\bar{\mathbf{v}}_0\right)-\bar{\mathbf{v}}_0^{(l)H}\mathbf{Q}_k\bar{\mathbf{v}}_0^{(l)}\right), \forall k, \quad (38b)$$

$$S_k \le 2\mathrm{Re}\left(\bar{\mathbf{v}}_1^{(l)H}\mathbf{Q}_k\bar{\mathbf{v}}_1\right)-\bar{\mathbf{v}}_1^{(l)H}\mathbf{Q}_k\bar{\mathbf{v}}_1^{(l)} \;\; \forall k, \quad (38c)$$

$$(34b),\ (34c), \quad (38d)$$

where (38) is a convex problem and thus it can be optimally solved by standard convex program solvers [43].

Algorithm 1 AO Algorithm

1: **Initialization**: Set iteration index to $l = 1$ and IRS BF vectors to $\bar{\mathbf{v}}_0 = \bar{\mathbf{v}}_0^{(1)}, \bar{\mathbf{v}}_1 = \bar{\mathbf{v}}_1^{(1)}$.
2: **repeat**
3: Solve problem (32) for given $\left\{\bar{\mathbf{v}}_0^{(l)}, \bar{\mathbf{v}}_1^{(l)}\right\}$ based on the interior point method and denote the optimal solution as $\Xi^{(l)} = \left\{\tau_0^{(l)}, \tau_{1,k}^{(l)}, p_k^{(l)}, f_k^{(l)}\right\}$.
4: Solve problem (38) for given $\Xi^{(l)}$ and $\left\{\bar{\mathbf{v}}_0^{(l)}, \bar{\mathbf{v}}_1^{(l)}\right\}$, where the optimal solution is denoted by $\left\{\bar{\mathbf{v}}_0^{(l+1)}, \bar{\mathbf{v}}_1^{(l+1)}\right\}$.
5: Update $l = l + 1$.
6: **until** the fractional increase of the objective value falls below a threshold $\xi > 0$.
7: Let $\left[\bar{\mathbf{v}}_0^l\right]_n = \left[\bar{\mathbf{v}}_0^l\right]_n / \left|\left[\bar{\mathbf{v}}_0^l\right]_n\right|$, $\left[\bar{\mathbf{v}}_1^l\right]_n = \left[\bar{\mathbf{v}}_1^l\right]_n / \left|\left[\bar{\mathbf{v}}_1^l\right]_n\right|$, and solve problem (32) for given $\left\{\bar{\mathbf{v}}_0^{(l)}, \bar{\mathbf{v}}_1^{(l)}\right\}$.

3) AO Algorithm Proposed for Solving $\left(\mathrm{P}_{\mathrm{TDMA}}^{\mathrm{case2}}\right)$ *:* An efficient AO algorithm where the IRS BF vectors and resource allocation are alternately optimized until convergence is achieved can be proposed. For arbitrary continuous amplitudes, the objective value of $(\mathrm{P}_{\mathrm{TDMA}}^{\mathrm{case2}})$ is non-decreasing by alternately optimizing $\{\tau_0, \tau_{1,k}, p_k, f_k\}$ and $\{\bar{\mathbf{v}}_0, \bar{\mathbf{v}}_1\}$, and also upper-bounded by a finite value. The proposed AO algorithm is guaranteed to converge when relaxing the unit-modulus constraints. Note that the converged solution, denoted by $\{\bar{\mathbf{v}}_0^*, \bar{\mathbf{v}}_1^*\}$, may not satisfy the unit-modulus constraints. In this case, the feasible IRS BF vectors, denoted by $\{\bar{\mathbf{v}}_0^\star, \bar{\mathbf{v}}_1^\star\}$, can be obtained as $[\bar{\mathbf{v}}_0^\star]_n = [\bar{\mathbf{v}}_0^*]_n / |[\bar{\mathbf{v}}_0^*]_n|$, $[\bar{\mathbf{v}}_1^\star]_n = [\bar{\mathbf{v}}_1^*]_n / |[\bar{\mathbf{v}}_1^*]_n|, \forall n$. Finally, problem (32) is solved for a given $\{\bar{\mathbf{v}}_0^\star, \bar{\mathbf{v}}_1^\star\}$ pair and

the feasible solution obtained for $\left(\mathrm{P}_{\mathrm{TDMA}}^{\mathrm{case2}}\right)$ is denoted by $\left\{\bar{\mathbf{v}}_0^\star, \bar{\mathbf{v}}_1^\star, \tau_0^\star, \tau_{1,k}^\star, p_k^\star, f_k^\star\right\}$. The details of the AO procedure are summarized in Algorithm 1.

It is worth noting that Algorithm 1 can be directly applied for obtaining the solution of $\left(\mathrm{P}_{\mathrm{TDMA}}^{\mathrm{case1}}\right)$ by setting $\mathbf{v}_1 = \mathbf{v}_0$. The details are omitted here for its simplicity.

4) Complexity Analysis: The computational complexity of Algorithm 1 is dominated by Step 3 and 4. Specifically, in Step 3, problem (32) can be solved by the interior-point method, whose complexity is $O\left((3K+1)^{3.5}\right)$ [43]. In Step 4, the complexity of solving problem (38) is $\mathcal{O}\left((2N)^{3.5}\right)$. Therefore, the total complexity of Algorithm 1 is $\mathcal{O}\left(L_{\mathrm{iter}}\left((2N)^{3.5}+(3K+1)^{3.5}\right)\right)$, where L_{iter} denotes the number of iterations for Algorithm 1.

B. Extension to Problem $\left(\mathrm{P}_{\mathrm{TDMA}}^{\mathrm{case3}}\right)$

In this subsection, we focus our attention on solving problem $\left(\mathrm{P}_{\mathrm{TDMA}}^{\mathrm{case3}}\right)$ for the scenario, where different IRS BF vectors can be adopted in different TSs where each device offloads its own tasks. It may be readily shown that the n-th phase shift of the optimal $\mathbf{v}_{1,k}^* = \left[e^{j\varphi_{1,k}^*}, \ldots, e^{j\varphi_{N,k}^*}\right]^T$ is given by

$$\varphi_{n,k}^* = \arg\left(h_{d,k}\right) + \arg\left(\left[\mathbf{q}_k\right]_n\right), n = 1, \ldots N. \tag{39}$$

After determining the optimal $\mathbf{v}_{1,k}^*$, we use $g_k^{\mathrm{off}} = \left|h_{d,k}^H + \mathbf{q}_k^H \mathbf{v}_1^{(k)*}\right|^2$ to represent the channel power gain of device k for the UL offloading link. Then, $\left(\mathrm{P}_{\mathrm{TDMA}}^{\mathrm{case3}}\right)$ is rewritten as follows

$$\max_{\tau_0, \tau_{1,k}, p_k, \mathbf{v}_0 f_k} \quad B\sum_{k=1}^{K} \tau_{1,k} \log_2\left(1 + \frac{p_k g_k^{\mathrm{off}}}{\sigma^2}\right) + \sum_{k=1}^{K} \frac{T f_k}{C} \tag{40a}$$

$$\text{s.t.} \quad \text{(10b)}, \ \text{(10c)}, \ \text{(10d)}, \ \text{(10e)}. \tag{40b}$$

Note that Algorithm 1 proposed in Section V-A can be directly applied to solving problem (40) with slight modifications. Specifically, for a fixed $\{\mathbf{v}_0\}$, the subproblem is simplified to problem (32), whose optimal solution can be efficiently solved by standard solvers. For the fixed $\{\tau_0, \tau_{1k}, p_k, f_k\}$, the subproblem with respect to $\{\mathbf{v}_0\}$ can be efficiently solved by exploiting the SCA technique proposed in Section V-A. The details are omitted here for brevity.

Remark 6: Although the individual rate constraint of each device is not considered in this paper, the proposed algorithm is applicable to the corresponding problems subject to such constraints. Specifically, for **Case 1**, the individual rate constraint of each device is given by

$$B\tau_{1,k}\log_2\left(1 + p_k \frac{\left|h_{d,k} + \mathbf{q}_k^H \mathbf{v}_0\right|^2}{\sigma^2}\right) + \frac{T f_k}{C} \geq R_{k,\min}, \ \ \forall k, \tag{41}$$

where $R_{k,\min}$ is the minimum number of computational bits required by device k. For any given $\mathbf{v}_0$, by letting $e_k = p_k \tau_{1,k}$, constraint (41) can be transformed to

$$B\tau_{1,k}\log_2\left(1 + \frac{e_k\left|h_{d,k} + \mathbf{q}_k^H \mathbf{v}_0\right|^2}{\tau_{1,k}\sigma^2}\right) + \frac{T f_k}{C} \geq R_{k,\min}, \ \ \forall k. \tag{42}$$

The left-hand-side of (42) is concave with respect to $\{e_k, \tau_{1,k}, f_k\}$. As such, (42) is convex and thus it can be handled by standard solvers. For a given $\{p_k, \tau_{1,k}, f_k\}$, (41) can be rewritten as

$$\left|h_{d,k} + \mathbf{q}_k^H \mathbf{v}_0\right|^2 \geq \frac{2^{\left(R_k^{\min} - T f_k / C\right)/(B\tau_{1,k})} - 1}{p_k}, \ \ \forall k. \tag{43}$$

The left-hand-side of (43) is convex with respect to $\mathbf{v}_0$ and thus it can be handled by the SCA technique proposed in Section V-A. Therefore, the proposed AO algorithm can be readily extended to solve the corresponding problem for **Case 1** subject to the individual rate constraint of each device. Replacing $\mathbf{v}_0$ by $\mathbf{v}_1$, the method is also applicable to solving the associated problem for **Case 2**. For **Case 3**, the optimal $\mathbf{v}_{1,k}$ is obtained in (39) and the resource allocation OP with respect to $\{p_k, \tau_{1,k}, f_k, \tau_0\}$ can be handled in a similar way.

Remark 7: Notice that although in this paper we consider the partial offloading, the design principles are also applicable to binary offloading [7], [9]. Actually, the proposed algorithm in this paper offers a heuristic method to determine the computational mode selection for binary offloading. For instance, for systems employing binary offloading, we adopt two mutually exclusive sets $\mathcal{K}_0$ and $\mathcal{K}_1$ to denote the indices of devices that operate in local computing and task offloading modes, respectively, such that $\mathcal{K}_0 \cup \mathcal{K}_1 = \{1, \ldots K\}$. The detailed method is described as follows:

First, the AO algorithm is adopted to solve the formulated optimization problems in this paper. Based on the obtained solutions, the ratio of the energy used for offloading of each device to its harvested energy can be computed as $m_k = p_k^\star \tau_k^\star \Big/ \left(\tau_0^\star P_E \left|h_{d,k} + \mathbf{q}_k^H \mathbf{v}_0^\star\right|^2\right)$. Then, we exploit the rounded result of m_k to indicate the computational mode for device k. Specifically, the device sets for $\mathcal{K}_0$ and $\mathcal{K}_1$ can be obtained as

$$\begin{aligned} \mathcal{K}_0 &= \left\{k : 0 \leq m_k < 0.5, k \in \{1, \ldots K\}\right\}, \\ \mathcal{K}_1 &= \left\{k : 0.5 \leq m_k \leq 0.5, k \in \{1, \ldots K\}\right\}, \end{aligned} \tag{44}$$

respectively. Given the obtained $\mathcal{K}_0$ and $\mathcal{K}_1$, the joint optimization of IRS BF and resource allocation can be solved by the algorithm proposed in this paper with slight modifications.

VI. Numerical Results

In this section, numerical results are provided for characterizing the performance of the proposed schemes and for gaining insights into the design and implementation of IRS-aided WP-MEC systems. The HAP and IRS are placed at $(0, 0, 0)$ m and $(10, 0, 3)$ m, respectively. The pathloss exponents of both the HAP-IRS and IRS-device channels are set to 2.2, while those of the HAP-device channels are set to 3. The signal attenuation at a reference distance of 1 m and noise power are set as 30 dB and $\sigma^2 = -75$ dBm, respectively. Furthermore, the bandwidth is set to $B = 200$ KHz since we consider narrow-band wireless systems. The system parameters related to the EH and computational model are set as follows: $\eta = 0.8$, $\gamma_c = 10^{-28}$, $C = [400, 800, 2000]$ cycles/bit and $T = 1$ s.

A. Activation Condition in Single-User Setup

To verify our analysis of the UL offloading activation condition in the single-user setup, we provide the following pair of numerical examples. The location of a typical device is

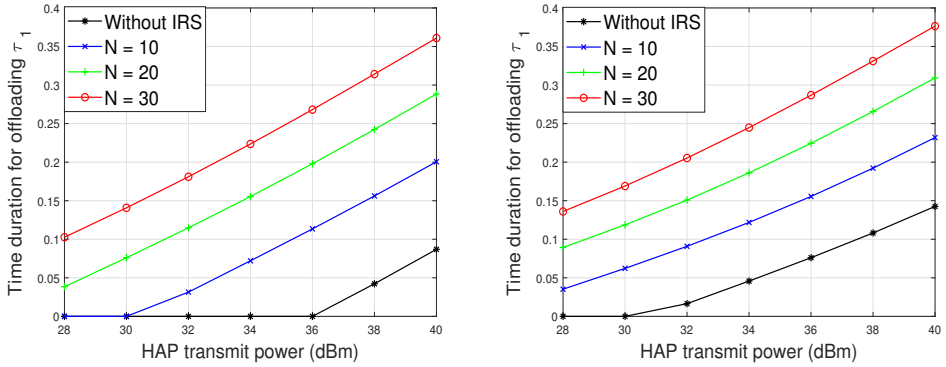

(a) $C = 400$ cycles/bit. (b) $C = 800$ cycles/bit.

Fig. 3. Illustration of UL offloading condition in pure LoS channel scenario.

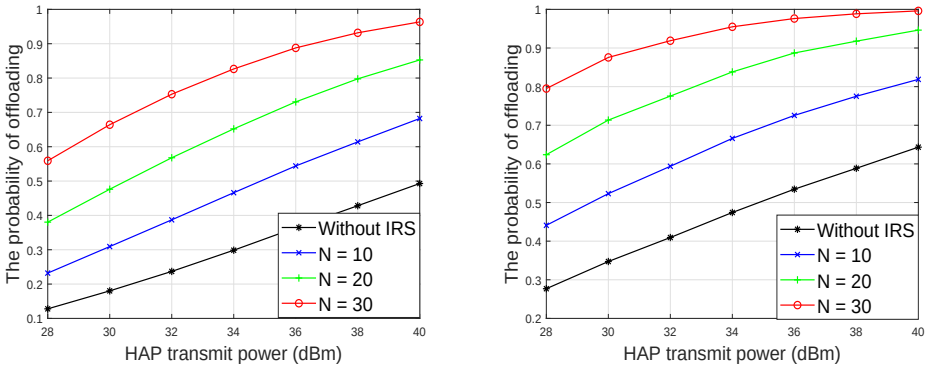

(a) $C = 400$ cycles/bit. (b) $C = 800$ cycles/bit.

Fig. 4. Illustration of UL offloading condition in general Rician channel scenario.

set to $(12, 0, 0)$ m. For the illustration of the optimal τ_1, we assume that all the links are LoS dominated, i.e., the Rician factor is high. The time allocated to UL offloading under $C = [400, 800]$ cycles/bit is presented in Fig. 3. The region where $\tau_1 > 0$ indicates that the UL offloading is activated. It can be observed that the transmit power P_E of the HAP which ensures $\tau_1 > 0$ decreases as N increases. This is consistent with Proposition 2, because the device is more likely to offload, when enjoying better channel conditions and the channel power gain can be improved by increasing the number of IRS elements N. Additionally, we can observe that the device tends to offload, when C becomes higher. This is because the computation rate attained by local computing becomes marginal at large C, which forces the device to offload more tasks for improving the computation rate. This is also consistent with (30), namely that the threshold used for activating UL offloading decreases as C increases.

To further verify the impact of the number of IRS elements on the offloading decisions of devices in random channels, we consider the setup that the small scale fading of all links follow Rician fading with a Rician factor of 3 dB. For $C = [400, 800]$ cycles/bit, the probability of the device chooses to offload versus the transmit power under different N is shown in Fig. 4. It is observed that the probability of offloading can be significantly improved by increasing the number of IRS elements, which validates that our analysis regarding the effectiveness of IRS for activating UL offloading is also applicable to general channel models.

B. Performance Comparison

Next, we consider a general multi-user setup to provide further performance comparisons and for demonstrating the efficiency of the proposed solutions. Specifically, five devices are uniformly and randomly distributed within a radius of 1.5 m centered at $(10, 0, 0)$ m. The small scale fading of all links is characterized by a Rician factor of 3 dB. We set $P_E = 40$ dBm in this subsection.

1) Efficiency of IRSs in WP-MEC Systems: To demonstrate the efficiency of IRSs in WP-MEC systems, the following benchmark schemes are considered for comparision: 1) Proposed AO in Algorithm 1 to solve $\left(\mathrm{P}_{\mathrm{TDMA}}^{\mathrm{case1}}\right)$; 2) Proposed AO in Algorithm 1 to solve $\left(\mathrm{P}_{\mathrm{TDMA}}^{\mathrm{case1}}\right)$ by ignoring the unit-modulus constraints; 3) Fixed WPT time but optimizing all other variables; 5) Fixed IRS phase shifts but optimizing all other variables; 4) Without IRS.

In Fig. 5(a), we plot the average total number of computed bits versus the number of IRS elements. It is observed that the average total number of computed bits output by our proposed Algorithm 1 over the benchmark schemes increases upon increasing N. In particular, the performance gap between "Proposed Algorithm 1" and "Relaxed unit modulus constraints" is small, which indicates that the performance loss incurred by using the relaxation method is negligible. Additionally, the performance gain of the scheme using the

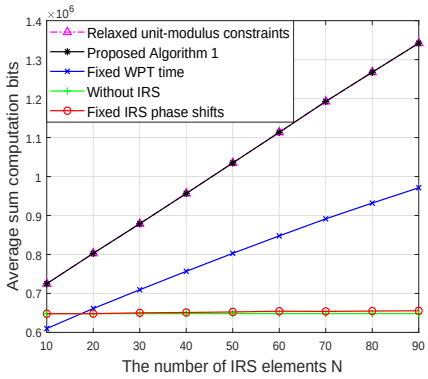

(a) Average sum computation rate versus N.

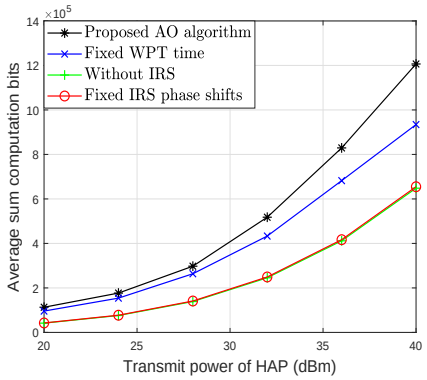

(b) Average sum computation rate versus P_E

Fig. 5. Performance Comparison with different schemes when $C = 2000$ cycles/bit and $N = 70$.

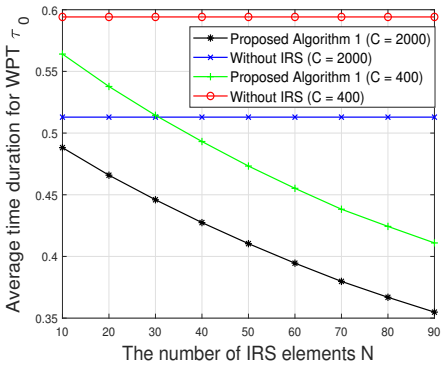

(a) Impact of N on WPT time.

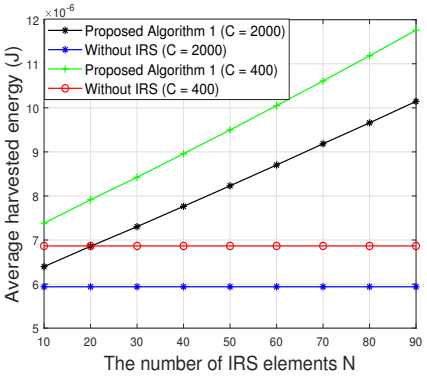

(b) Impact of N on the harvested energy.

Fig. 6. Impact of N on WPT time and harvested energy.

fixed phase shifts over the system without IRS is marginal, which highlights the importance of carefully designing the IRS BF. Moreover, for small N, the scheme using fixed WPT duration performs even worse than that without IRS, but for large N, it significantly outperforms the fixed phase shifts-based scheme. This demonstrates that the gain of IRS BF compensates the performance loss due to a fixed WPT duration. Nevertheless, the results unveil the importance of the joint design of the WPT duration and IRS BF. In Fig. 5(b), we plot the average total number of computed bits versus P_E. It can be observed that our proposed design outperforms a range of benchmark schemes and the performance gap is enlarged as the HAP transmit power increases, which further demonstrates the importance of jointly designing the WPT duration and the IRS BF.

To further demonstrate the benefits brought out by IRSs for WP-MEC systems, we investigate the impact of N both on the DL WPT duration and on the total energy harvested at each device. As shown in Fig. 6(a), the optimized WPT duration decreases with N for both $C = 400$ and $C = 2000$, which indicates that the energy consumed at the HAP, namely $E_{\rm HAP} = \tau_0 P_E$, can be reduced by increasing N. Meanwhile, more time can be reserved for each device's UL offloading, which increases the total number of computed bits. This implies that embedding IRSs into WP-MEC systems achieves both computation rate improvements and energy consumption reductions. Although a higher N leads to a reduced DL WPT time τ_0, Fig. 6(b) shows that the total energy harvested by each device even increases with N. This is because the energy signal reflected by the IRS towards devices becomes more focused, which in turn improves the efficiency of WPT upon increasing N. Indeed, the high passive BF gain attained by IRSs increases the degrees of freedom for enhancing the flexibility of resource allocation design. Thanks to the improved channel conditions granted for both the DL WPT and UL offloading links, more time is available for offloading, while maintaining sufficient harvested energy, which achieves substantial computation rate improvements.

2) Comparison of Different Computational Modes: For comparison, we consider different computational modes as follows: 1) The partial offloading mode: Algorithm 1 is applied for solving $\left(\mathrm{P}_{\mathrm{TDMA}}^{\mathrm{case1}}\right)$; 2) Offloading only: The algorithm proposed in [38] is adopted for solving the resultant problem, when all devices only perform UL offloading; 3) Local computing only: All the devices only perform local computing and $\mathbf{v}_0$ is optimized based on the method in Section V-A. The average total number of computed bits versus N is plotted in Fig. 7 for different values of C. As expected, the partial offloading mode performs the best among all the specific schemes. The reason for this trend is that all the devices can flexibly select their computational mode based on the specific channel conditions under the partial offloading mode. Additionally, the offloading only mode significantly outperforms the local computing mode. This is because the IRS can only benefit the DL WPT for local computing mode, while the efficiency of both DL WPT and UL offloading can be improved with the aid of IRSs for the

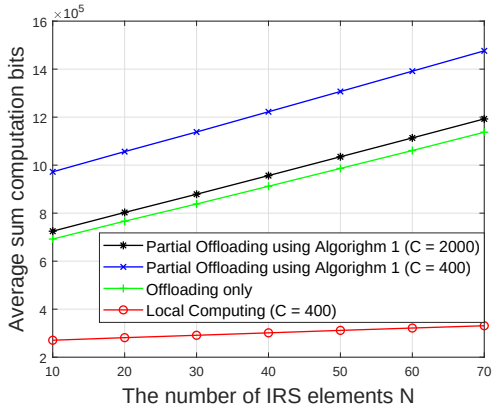

Fig. 7. Performance comparison of different computation modes.

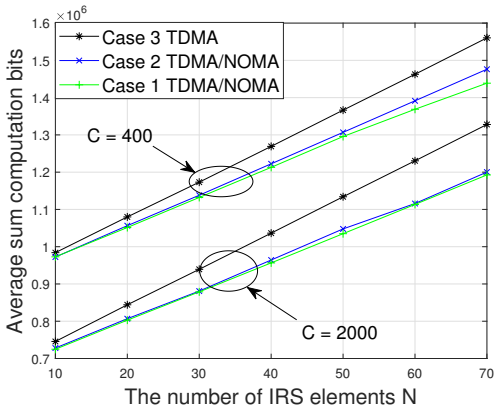

Fig. 8. Performance comparison of different DIBF schemes.

offloading-only mode. Moreover, it is observed that the gain of partial offloading mode over the offloading only-mode becomes marginal for large C, since the number of bits computed locally is low for a high C.

3) Impact of DIBF: To illustrate the impact of DIBF on the computation rate, the average total number of computed bits versus N is presented in Fig. 8 for three cases. Note that the performance of NOMA is the same as that of TDMA for both **Case 1** and **Case 2**. It is observed in Fig. 8 that the computation rate difference between **Case 3** and **Case 1/Case 2** expands as N increases, which highlights the potential benefits of using dynamic IRS BF in TDMA-based UL offloading. The results reveal that the performance of TDMA may in fact become better than NOMA by using different IRS BF vectors for UL offloading in IRS-aided WP-MEC systems. Additionally, the performance gain of **Case 3** over **Case 1/Case 2** becomes more significant, when C is high. This is because using dedicated IRS BF vectors for UL offloading only improves the computation rate contributed by UL offloading, but has no effect on local computing. Furthermore, for high C, the computation rate is dominated by that of UL offloading, while that of local computing is negligible. Finally, **Case 2** only attains a marginal gain over **Case 1**, especially for high C, which is in line with our analysis in Remark 2. The results suggest that using the same IRS BF vector is appropriate for both the DL WPT and UL offloading in scenarios, where the devices have weak computing capability and/or the system is sensitive to the signaling overhead.

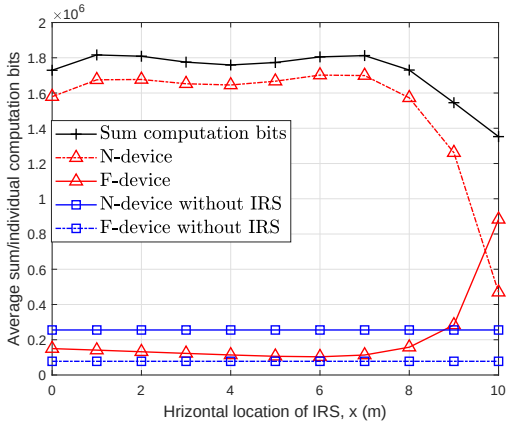

Fig. 9. Sum/invidual device computation rate versus IRSs horizontal location when $N = 70$ and $C = 2000$ cycles/bit.

C. Deployment of IRS for Doubly-Near-far Problem

Note that the "doubly-near-far effect" is a critical issue in wireless-powered communication systems. For our considered WP-MEC system, the device which is located far away from the HAP would generally harvest less energy through the DL WPT but it may require more energy to perform UL offloading than that of a device close to the HAP. Therefore, the computation rate of a distant device may be significantly lower than that of a nearby device, which leads to the severe user unfair issue. Fortunately, this issue can be readily mitigated by the appropriate deployment of the IRS. To illustrate this, we consider a setup, where the two devices, namely the near device (*N-device*) and the far device (*F-device*), are located at $(7, 0, 0)$ m and $(10, 0, 0)$ m, respectively. The IRS is located at $(x, 0, 3)$ m. We show in Fig. 9 the individual devices' computation rate versus the horizontal coordinate of the IRS, i.e., x. It can observed that the computation rate of the *N-device* is significantly higher than that of the *F-device* without IRS. By contrast, when deploying the IRS near to *F-device*, the computation rate of the *F-device* approaches that of the *N-device* and can be even higher than that of the *N-device*, when $x = 10$ m. Thanks to the ability of the IRS to reconfigure the wireless channels, the computation rates of the two devices can be well comprised and become much higher than those in the absence of the IRS. The result demonstrates the benefits of deploying the IRS for resolving the rate fairness issue imposed by the "doubly-near-far" effect.

VII. Conclusion

The achievable computation rate performance of IRS-aided WP-MEC systems was studied in this paper. By taking into account the interplay between IRSs and the MA schemes, we answered a fundamental question: Does NOMA improve the achievable computation rate of IRS-aided WP-MEC systems compared to traditional TDMA? We first unveiled that offloading adopting a TDMA scheme achieves a better computation rate than that of NOMA, when the IRS BF vector can be flexibly adapted for UL offloading. The conclusions are quite different from the previous works regarding conventional MEC systems, e.g., [10]–[13]. The obtained results provide important guidelines for selecting MA schemes for UL offloading in IRS-aided WP-MEC systems: it is preferable to exploit TDMA instead of NOMA for improving computation rate at the cost

of extra signaling overhead. Furthermore, we proposed computationally efficient algorithms for maximizing computation rate under different DIBF schemes. Our numerical results validated the efficiency of our design over the benchmark schemes and also confirmed the benefits of IRSs in WP-MEC systems under different setups. In our future work, it is worth investigating the effectiveness of different MA schemes in relevant MEC systems by considering the impact of IRS in terms of other performance metrics, such as latency, power consumption, energy efficiency, etc.

Appendix A: Proof of Theorem 1

The key idea of the proof for Theorem 1 lies in the following two aspects. First, based on the arbitrary solution of TDMA, we can always construct a solution for NOMA which achieves the same objective value as that of TDMA and thus it indicates that the optimal value of NOMA is no smaller than that of TDMA. Second, based the arbitrary solution of NOMA, a solution of TDMA can be always constructed which achieves the same objective value as that of NOMA and thus it indicates that the optimal value of TDMA is no smaller than that of NOMA. The detailed procedures are as follows:

The proof starts by showing that $R^{\text{case2}}_{\text{TDMA}} \leq R^{\text{case2}}_{\text{NOMA}}$. We denote the set characterizing the devices whose UL offloading is activated as $\mathcal{K}_{\text{off}}$. Given that $\mathbf{v}_0 = \mathbf{v}_0^*, \mathbf{v}_1 = \mathbf{v}_1^*, f_k = f_k^*$ for $(\text{P}^{\text{case2}}_{\text{TDMA}})$, the optimal p_k can be expressed as $p_k^* = \left(\tau_0 \eta P_E \left|h_{d,k} + \mathbf{q}_k^H \mathbf{v}_0^*\right|^2 - T\gamma_c f_k^{*3}\right)(\tau_{1,k})^{-1}$ for $k \in \mathcal{K}_{\text{off}}$, because each device will deplete all of its energy. Now, we first discuss some properties of $\tau_{1,k}^*$ and τ_0^*. To this end, $(\text{P}^{\text{case2}}_{\text{TDMA}})$ can be simplified by optimizing τ_0 and $\tau_{1,k}$ as follows:

$$\max_{\tau_{1,k},\tau_0} \; B \sum_{k\in\mathcal{K}_{\text{off}}} \tau_{1,k} \log_2\left(1 + f_k\left(\tau_0, \tau_{1,k}\right)\right) \tag{45a}$$

$$\text{s.t.} \;\; (10c), \tag{45b}$$

where

$$f_k\left(\tau_0, \tau_{1,k}\right) = \frac{\tau_0 \eta P_E \left|h_{d,k} + \mathbf{q}_k^H \mathbf{v}_0^*\right|^2 - T\gamma_c f_k^{*3}}{\tau_{1,k}\sigma^2} \left|h_{d,k} + \mathbf{q}_k^H \mathbf{v}_1^*\right|^2. \tag{46}$$

Note that problem (45) is a convex problem and its Lagrangian function is

$$\mathcal{L}_{(\text{TDMA})}\left(\tau_0, \tau_{1,k}, \lambda\right) = B \sum_{k\in\mathcal{K}_{\text{off}}} \tau_{1,k} \log_2\left(1 + f_k\left(\tau_0, \tau_{1,k}\right)\right) + \lambda\left(T - \tau_0 - \sum_{k=1}^{K} \tau_{1,k}\right), \tag{47}$$

where $\lambda \geq 0$ is the dual variable associated with (45b). According to the Karush-Kuhn-Tucker (KKT) conditions, we have

$$\frac{\partial \mathcal{L}_{(\text{TDMA})}\left(\tau_0, \tau_{1,k}, \lambda\right)}{\partial \tau_{1,k}} = B\left(\log_2\left(1+\Gamma_k\right) - \frac{\Gamma_k}{\left(1+\Gamma_k\right)\ln 2}\right) - \lambda \triangleq M\left(\Gamma_k\right) = 0, \tag{48}$$

$$\frac{\partial \mathcal{L}_{(\text{TDMA})}\left(\tau_0, \tau_{1,k}, \lambda\right)}{\partial \tau_0} = B\frac{\tau_0 \eta P_E \left|h_{d,k} + \mathbf{q}_k^H \mathbf{v}_0^*\right|^2 \left|h_{d,k} + \mathbf{q}_k^H \mathbf{v}_1^*\right|^2}{\sigma^2\left(1+\Gamma_k\right)\ln 2} - \lambda = 0, \tag{49}$$

where

$$\Gamma_k = \frac{\tau_0 \eta P_E \left|h_{d,k} + \mathbf{q}_k^H \mathbf{v}_0^*\right|^2 - T\gamma_c f_k^{*3}}{\tau_{1,k}\sigma^2} \left|h_{d,k} + \mathbf{q}_k^H \mathbf{v}_1^*\right|^2 \tag{50}$$

denotes the received signal-to-noise ratio (SNR) of device k. Since $M\left(\Gamma_k\right)$ is an increasing function with respect to Γ_k, each device shares the same SNR at the optimal solution, i.e., $\Gamma_k = \Gamma_m = \Gamma^*, \forall k, m$. In particular, Γ^* is the solution of the equation:

$$H\left(\Gamma\right) \triangleq \log_2\left(1+\Gamma\right) - \frac{\Gamma}{\left(1+\Gamma\right)\ln 2} - \frac{\eta P_E \left|h_{d,k} + \mathbf{q}_k^H \mathbf{v}_0^*\right|^2 \left|h_{d,k} + \mathbf{q}_k^H \mathbf{v}_1^*\right|^2}{\sigma^2\left(1+\Gamma\right)\ln 2} = 0, \tag{51}$$

which can be readily obtained by applying the bisection search method, since $H\left(\Gamma\right)$ is an increasing function with respect to Γ. Accordingly, $\tau_{1,k}^*$ and τ_0^* are given by

$$\tau_0^* = \frac{T + \sum_{k\in\mathcal{K}_{\text{off}}} \frac{T\gamma_c f_k^{*3}\left|h_{d,k}+\mathbf{q}_k^H \mathbf{v}_1^*\right|^2}{\Gamma^*\sigma^2}}{1 + \sum_{k\in\mathcal{K}_{\text{off}}} \frac{\eta P_E \left|h_{d,k}+\mathbf{q}_k^H \mathbf{v}_0^*\right|^2 \left|h_{d,k}+\mathbf{q}_k^H \mathbf{v}_1^*\right|^2}{\Gamma^*\sigma^2}},$$

$$\tau_{1,k}^* = \frac{\tau_0^* \eta P_E \left|h_{d,k} + \mathbf{q}_k^H \mathbf{v}_0^*\right|^2 - T\gamma_c f_k^{*3}}{\Gamma^*\sigma^2 \left|h_{d,k} + \mathbf{q}_k^H \mathbf{v}_1^*\right|^{-2}}, \tag{52}$$

respectively. Since $\Gamma_k = \Gamma_m = \Gamma^*, \forall k, m$, the optimal value of $(\text{P}^{\text{case2}}_{\text{TDMA}})$ can be rewritten as (53) shown at the top of the next page, where $\tau_1^* = \sum_{k\in\mathcal{K}_{\text{off}}} \tau_{1,k}^*$. It is plausible that $\{\tau_0^*, \tau_1^*, p_k^*, \mathbf{v}_0^*, \mathbf{v}_1^*, f_k^*\}$ is a feasible solution for $(\text{P}^{\text{case2}}_{\text{NOMA}})$, which yields $R^{\text{case2}}_{\text{TDMA}} \leq R^{\text{case2}}_{\text{NOMA}}$.

Next, we show that $R^{\text{case2}}_{\text{TDMA}} \geq R^{\text{case2}}_{\text{NOMA}}$. At the optimal solution of $(\text{P}^{\text{case2}}_{\text{NOMA}})$, we can always construct a new solution satisfying $\tilde{\tau}_0 = \tau_0^\star, \sum_{k\in\mathcal{K}_{\text{off}}} \tilde{\tau}_{1,k} = \tau_1^\star$, so that all devices share the same received SNR in the TDMA case, i.e.,

$$\frac{\left(\tilde{\tau}_0 \eta P_E \left|h_{d,k} + \mathbf{q}_k^H \mathbf{v}_0^\star\right|^2 - T\gamma_c (f_k^\star)^3\right)}{\tilde{\tau}_{1,k}\sigma^2 \left|h_{d,k} + \mathbf{q}_k^H \mathbf{v}_1^\star\right|^{-2}} = \frac{\left(\tilde{\tau}_0 \eta P_E \left|h_{d,m} + \mathbf{q}_m^H \mathbf{v}_0^\star\right|^2 - T\gamma_c (f_m^\star)^3\right)}{\tilde{\tau}_{1,m}\sigma^2 |h_{d,m} + \mathbf{q}_m^H \mathbf{v}_1^\star|^{-2}}, \forall k \neq m. \tag{55}$$

It is easy to verify that $\{\tilde{\tau}_0, \tilde{\tau}_{1,k}, \forall k\}$ is also feasible for $(\text{P}^{\text{case2}}_{\text{TDMA}})$ and always exists, which yields (54) shown at the top of the next page, where (a) follows that $\sum_{k\in\mathcal{K}_{\text{off}}} \tilde{\tau}_{1,k} = \tau_1^\star$ and all devices share the same SNR at the constructed solution. At the optimal solution of $(\text{P}^{\text{case2}}_{\text{TDMA}})$, it follows that $R^{\text{case2}}_{\text{TDMA}} \geq R^{\text{case2}}_{\text{NOMA}}$.

Given $R^{\text{case2}}_{\text{TDMA}} \leq R^{\text{case2}}_{\text{NOMA}}$ and $R^{\text{case2}}_{\text{TDMA}} \geq R^{\text{case2}}_{\text{NOMA}}$, we have $R^{\text{case2}}_{\text{TDMA}} = R^{\text{case2}}_{\text{NOMA}}$, which thus completes the proof.

Appendix B: Proof of Proposition 1

Assume that the optimal solution of problem (21) is $\{\tau_0^*, \tau_1^*, f^*, e^*\}$, where $\tau_1^* > 0$ indicates that UL offloading should be activated for maximizing the computation rate. By contrast, the device would only perform local computing if $\tau_1^* = 0$.

We first consider the case that $\tau_1^* > 0$. Then, the optimal solution $\{\tau_0^*, \tau_1^*, f^*, e^*\}$ can be derived by analyzing the partial

$$R_{\mathrm{TDMA}}^{\mathrm{case2}}=B\tau_1^*\log_2\left(1+\frac{\sum_{k\in\mathcal{K}_{\mathrm{off}}}\left(\tau_0^*\eta P_E\left|h_{d,k}+\mathbf{q}_k^H\mathbf{v}_0^*\right|^2-T\gamma_c f_k^{*3}\right)\left|h_{d,k}+\mathbf{q}_k^H\mathbf{v}_1^*\right|^2}{\tau_1^*\sigma^2}\right)+\sum_{k=1}^{K}\frac{Tf_k^*}{C}, \tag{53}$$

$$\begin{aligned}\tilde{R}_{\mathrm{TDMA}}^{\mathrm{case2}} &= B\sum_{k\in\mathcal{K}_{\mathrm{off}}}\tilde{\tau}_{1,k}\log_2\left(1+\frac{\tilde{\tau}_0\eta P_E\left|h_{d,k}+\mathbf{q}_k^H\mathbf{v}_0^\star\right|^2-T\gamma_c(f_k^\star)^3}{\tilde{\tau}_{1,k}\sigma^2}\left|h_{d,k}+\mathbf{q}_k^H\mathbf{v}_1^\star\right|^2\right)+\sum_{k=1}^{K}\frac{Tf_k^\star}{C}\\ &\overset{(a)}{=} B\tau_1^\star\log_2\left(1+\frac{\sum_{k\in\mathcal{K}_{\mathrm{off}}}\left(\tilde{\tau}_0\left|h_{d,k}+\mathbf{q}_k^H\mathbf{v}_0^\star\right|^2-T\gamma_c(f_k^\star)^3\right)\left|h_{d,k}+\mathbf{q}_k^H\mathbf{v}_1^\star\right|^2}{\tau_1^\star\sigma^2}\right)+\sum_{k=1}^{K}\frac{Tf_k^\star}{C}\\ &=R_{\mathrm{NOMA}}^{\mathrm{case2}},\end{aligned} \tag{54}$$

Lagrangian function of problem (21), which can be written as

$$\begin{aligned}\mathcal{L}(\Xi)=&B\tau_1\log_2\left(1+\frac{eh}{\tau_1\sigma^2}\right)+\frac{Tf}{C}+\mu\left(T-\tau_0-\tau_1\right)\\&+\lambda\left(\eta\tau_0P_Eh-e_1-T\gamma_cf_1^3\right),\end{aligned} \tag{56}$$

where $\Xi=\{\tau_0,\tau_1,e,f,\lambda,u\}$, $\lambda\geq 0$ and $\mu\geq 0$ are the corresponding Lagrange multipliers. Since problem (21) is convex, its optimal solution can be obtained through analyzing the KKT conditions. Taking the partial derivative of $\mathcal{L}(\Xi)$ with respect to τ_1, τ_0, e, and f, respectively, we have

$$\frac{\partial\mathcal{L}(\Xi)}{\partial\tau_1}=B\log_2\left(1+\frac{eh}{\tau_1\sigma^2}\right)-\frac{Beh}{(\tau_1\sigma^2+eh)\ln 2}-u, \tag{57}$$

$$\frac{\partial\mathcal{L}(\Xi)}{\partial\tau_0}=\lambda\eta P_Eh-u, \tag{58}$$

$$\frac{\partial\mathcal{L}(\Xi)}{\partial e}=\frac{B\tau_1h}{(\tau_1\sigma^2+eh)\ln 2}-\lambda, \tag{59}$$

$$\frac{\partial\mathcal{L}(\Xi)}{\partial f}=\frac{T}{C}-3\lambda T\gamma_cf. \tag{60}$$

In this case, UL offloading is activated at the optimal solution, i.e., $\tau_1^*>0, e_1^*>0$. Furthermore, $\tau_0^*>0$ always holds at the optimal solution. Therefore, we have $\frac{\partial\mathcal{L}(\Xi)}{\partial\tau_0^*}=0$, $\frac{\partial\mathcal{L}(\Xi)}{\partial\tau_1^*}=0$, $\frac{\partial\mathcal{L}(\Xi)}{\partial e^*}=0$, and $\frac{\partial\mathcal{L}(\Xi)}{\partial f^*}=0$. After some further algebraic operations, $p^*=e^*/\tau_1^*$ satisfies

$$\log_2\left(1+\frac{p^*h}{\sigma^2}\right)-\frac{p^*h}{(\sigma^2+p^*h)\ln 2}-\frac{\eta P_Eh^2}{(\sigma^2+p^*h)\ln 2}=0, \tag{61}$$

which yields (30) and can be obtained by bisection search. Accordingly, f^* is given by

$$f^*=\sqrt{\frac{1}{3C\lambda^*\gamma_c}}=\sqrt{\frac{(\sigma^2+p^*h)\ln 2}{3Ch\gamma_cB}}. \tag{62}$$

Since the device depletes all of its harvested energy and $\tau_0^*+\tau_1^*=T$, we have

$$\tau_1^*=\frac{\eta P_Eh-\gamma_c\left(\frac{\left(\sigma^2+p^*h\right)\ln 2}{3Ch\gamma_cB}\right)^{\frac{3}{2}}}{p^*+\eta P_Eh}T, \tau_0^*=T-\tau_1^*. \tag{63}$$

According to (63), it can be observed that $\tau_1^*>0$ always holds if $\eta P_Eh>\gamma_c\left(\frac{\left(\sigma^2+p^*h\right)\ln 2}{3Ch\gamma_cB}\right)^{\frac{3}{2}}$. Thus, (23) serves as the UL offloading activation condition. Under the condition of (23), the optimal solution for problem (21) is

$$f^*=\sqrt{\frac{(\sigma^2+p^*h)\ln 2}{3Ch\gamma_cB}}, \tau_1^*=\frac{\eta P_Eh-\gamma_c\left(\frac{\left(\sigma^2+p^*h\right)\ln 2}{3Ch\gamma_cB}\right)^{\frac{3}{2}}}{p^*+\eta P_Eh}T,$$
$$\tau_0^*=T-\tau_1^*, e^*=\tau_1^*p^*. \tag{64}$$

For the scenario of $\eta P_Eh<\gamma_c\left(\frac{\left(\sigma^2+p^*h\right)\ln 2}{3Ch\gamma_cB}\right)^{\frac{3}{2}}$, i.e., (23) is not satisfied, the UL offloading is not activated. The optimal solution of problem (21) is given by

$$\tau_0^*=T, \tau_1^*=0, f^*=\left(\frac{P_E\eta h}{\gamma_c}\right)^{1/3}, e^*=0. \tag{65}$$

REFERENCES

[1] G. Chen and Q. Wu, "Computation Rate Maximization for IRS-aided Wireless Powred MEC Systems," *in Proc. IEEE Wireless Communications and Networking Conference (WCNC) Workshops, Austin, Apr. 2022*.

[2] L. Chettri and R. Bera, "A Comprehensive Survey on Internet of Things (IoT) Toward 5G Wireless Systems," *IEEE Internet Things J.*, vol. 7, no. 1, pp. 16–32, Jan. 2020.

[3] Z. Ding, X. Lei, G. K. Karagiannidis, R. Schober, J. Yuan, and V. K. Bhargava, "A Survey on Non-Orthogonal Multiple Access for 5G Networks: Research Challenges and Future Trends," *IEEE J. Sel. Areas Commun.*, vol. 35, no. 10, pp. 2181–2195, Oct. 2017.

[4] Y. Mao, C. You, J. Zhang, K. Huang, and K. B. Letaief, "A Survey on Mobile Edge Computing: The Communication Perspective," *IEEE Commun. Surveys Tuts.*, vol. 19, no. 4, pp. 2322–2358, Apr. 2017.

[5] C. You, K. Huang, and H. Chae, "Energy Efficient Mobile Cloud Computing Powered by Wireless Energy Transfer," *IEEE J. Sel. Areas Commun.*, vol. 34, no. 5, pp. 1757–1771, May 2016.

[6] F. Wang, "Computation Rate Maximization for Wireless Powered Mobile Edge Computing," in *Proc. 23rd Asia-Pacific Conf. Commun., Perth, WA, Australia*, Dec. 2017, pp. 1–6.

[7] S. Bi and Y. J. Zhang, "Computation Rate Maximization for Wireless Powered Mobile-Edge Computing With Binary Computation Offloading," *IEEE Trans. Wireless Commun.*, vol. 17, no. 6, pp. 4177–4190, Jun. 2018.

[8] F. Zhou, Y. Wu, R. Q. Hu, and Y. Qian, "Computation Rate Maximization in UAV-Enabled Wireless-Powered Mobile-Edge Computing Systems," *IEEE J. Sel. Areas Commun.*, vol. 36, no. 9, pp. 1927–1941, Sep. 2018.

[9] J. Liu, K. Xiong, D. W. K. Ng, P. Fan, Z. Zhong, and K. B. Letaief, "Max-Min Energy Balance in Wireless-Powered Hierarchical Fog-Cloud Computing Networks," *IEEE Trans. Wireless Commun.*, vol. 19, no. 11, pp. 7064–7080, Nov. 2020.

[10] F. Zhou and R. Q. Hu, "Computation Efficiency Maximization in Wireless-Powered Mobile Edge Computing Networks," *IEEE Trans. Wireless Commun.*, vol. 19, no. 5, pp. 3170–3184, May. 2020.

[11] L. Shi, Y. Ye, X. Chu, and G. Lu, "Computation Energy Efficiency Maximization for a NOMA Based WPT-MEC Network," *IEEE Internet Things J.*, pp. 1–1, Jul. 2021.

[12] F. Wang, J. Xu, and Z. Ding, "Multi-Antenna NOMA for Computation Offloading in Multiuser Mobile Edge Computing Systems," *IEEE Trans. Commun.*, vol. 67, no. 3, pp. 2450–2463, Mar. 2019.

[13] F. Fang, Y. Xu, Z. Ding, C. Shen, M. Peng, and G. K. Karagiannidis, "Optimal Resource Allocation for Delay Minimization in NOMA-MEC Networks," *IEEE Trans. Commun.*, vol. 68, no. 12, pp. 7867–7881, Dec. 2020.

[14] F. Wang, J. Xu, X. Wang, and S. Cui, "Joint Offloading and Computing Optimization in Wireless Powered Mobile-Edge Computing Systems," *IEEE Trans. Wireless Commun.*, vol. 17, no. 3, pp. 1784–1797, Mar. 2018.

[15] E. Boshkovska, D. W. K. Ng, N. Zlatanov, A. Koelpin, and R. Schober, "Robust Resource Allocation for MIMO Wireless Powered Communication Networks Based on a Non-Linear EH Model," *IEEE Trans. Commun.*, vol. 65, no. 5, pp. 1984–1999, May. 2017.

[16] J. Hu, K. Yang, G. Wen, and L. Hanzo, "Integrated Data and Energy Communication Network: A Comprehensive Survey," *IEEE Commun. Surveys Tuts.*, vol. 20, no. 4, pp. 3169–3219, Apr. 2018.

[17] G. N. Kamga and S. Aissa, "Wireless Power Transfer in mmWave Massive MIMO Systems With/Without Rain Attenuation," *IEEE Trans. Commun.*, vol. 67, no. 1, pp. 176–189, Jan. 2019.

[18] M. Zeng, W. Hao, O. A. Dobre, and H. V. Poor, "Delay Minimization for Massive MIMO Assisted Mobile Edge Computing," *IEEE Trans. Veh. Technol.*, vol. 69, no. 6, pp. 6788–6792, Jun. 2020.

[19] M. Di Renzo, A. Zappone, M. Debbah, M.-S. Alouini, C. Yuen, J. de Rosny, and S. Tretyakov, "Smart Radio Environments Empowered by Reconfigurable Intelligent Surfaces: How It Works, State of Research, and The Road Ahead," *IEEE J. Sel. Areas Commun.*, vol. 38, no. 11, pp. 2450–2525, Nov. 2020.

[20] Q. Wu and R. Zhang, "Towards Smart and Reconfigurable Environment: Intelligent Reflecting Surface Aided Wireless Network," *IEEE Commun. Mag.*, vol. 58, no. 1, pp. 106–112, Jan. 2020.

[21] Q. Wu, S. Zhang, B. Zheng, C. You, and R. Zhang, "Intelligent Reflecting Surface-Aided Wireless Communications: A Tutorial," *IEEE Trans. Commun.*, vol. 69, no. 5, pp. 3313–3351, May 2021.

[22] C. Huang, A. Zappone, G. C. Alexandropoulos, M. Debbah, and C. Yuen, "Reconfigurable Intelligent Surfaces for Energy Efficiency in Wireless Communication," *IEEE Trans. Wireless Commun.*, vol. 18, no. 8, pp. 4157–4170, Aug. 2019.

[23] Q. Wu and R. Zhang, "Intelligent Reflecting Surface Enhanced Wireless Network via Joint Active and Passive Beamforming," *IEEE Trans. Wireless Commun.*, vol. 18, no. 11, pp. 5394–5409, Nov. 2019.

[24] X. Mu, Y. Liu, L. Guo, J. Lin, and N. Al-Dhahir, "Exploiting Intelligent Reflecting Surfaces in NOMA Networks: Joint Beamforming Optimization," *IEEE Trans. Wireless Commun.*, vol. 19, no. 10, pp. 6884–6898, Oct. 2020.

[25] C. Huang, R. Mo, and C. Yuen, "Reconfigurable Intelligent Surface Assisted Multiuser MISO Systems Exploiting Deep Reinforcement Learning," *IEEE J. Sel. Areas Commun.*, vol. 38, no. 8, pp. 1839–1850, Aug. 2020.

[26] M. Hua, Q. Wu, D. W. K. Ng, J. Zhao, and L. Yang, "Intelligent Reflecting Surface-Aided Joint Processing Coordinated Multipoint Transmission," *IEEE Trans. Commun.*, vol. 69, no. 3, pp. 1650–1665, Mar. 2021.

[27] Y. Yang, B. Zheng, S. Zhang, and R. Zhang, "Intelligent Reflecting Surface Meets OFDM: Protocol Design and Rate Maximization," *IEEE Trans. Commun.*, vol. 68, no. 7, pp. 4522–4535, Jul. 2020.

[28] S. Zhang and R. Zhang, "Intelligent Reflecting Surface Aided Multi-User Communication: Capacity Region and Deployment Strategy," *IEEE Trans. Commun.*, vol. 69, no. 9, pp. 5790–5806, Sep. 2021.

[29] Q. Wu and R. Zhang, "Beamforming Optimization for Wireless Network Aided by Intelligent Reflecting Surface With Discrete Phase Shifts," *IEEE Trans. Commun.*, vol. 68, no. 3, pp. 1838–1851, Mar. 2020.

[30] K. Zhi, C. Pan, H. Ren, and K. Wang, "Uplink Achievable Rate of Intelligent Reflecting Surface-Aided Millimeter-Wave Communications With Low-Resolution ADC and Phase Noise," *IEEE Wireless Commun. Lett.*, vol. 10, no. 3, pp. 654–658, Jun. 2021.

[31] S. Abeywickrama, R. Zhang, Q. Wu, and C. Yuen, "Intelligent Reflecting Surface: Practical Phase Shift Model and Beamforming Optimization," *IEEE Trans. Commun.*, vol. 68, no. 9, pp. 5849–5863, Sep. 2020.

[32] Q. Wu, X. Guan, and R. Zhang, "Intelligent Reflecting Surface-Aided Wireless Energy and Information Transmission: An Overview," *Proceedings of the IEEE*, vol. 110, no. 1, pp. 150–170, Jan. 2022.

[33] Q. Wu and R. Zhang, "Weighted Sum Power Maximization for Intelligent Reflecting Surface Aided SWIPT," *IEEE Wireless Commun. Lett.*, vol. 9, no. 5, pp. 586–590, Oct. 2020.

[34] S. Zargari, A. Khalili, and R. Zhang, "Energy Efficiency Maximization via Joint Active and Passive Beamforming Design for Multiuser MISO IRS-Aided SWIPT," *IEEE Wireless Commun. Lett.*, vol. 10, no. 3, pp. 557–561, Jun. 2021.

[35] Q. Wu and R. Zhang, "Joint Active and Passive Beamforming Optimization for Intelligent Reflecting Surface Assisted SWIPT Under QoS Constraints," *IEEE J. Sel. Areas Commun.*, vol. 38, no. 8, pp. 1735–1748, Aug. 2020.

[36] B. Lyu, P. Ramezani, D. T. Hoang, S. Gong, Z. Yang, and A. Jamalipour, "Optimized Energy and Information Relaying in Self-Sustainable IRS-Empowered WPCN," *IEEE Trans. Commun.*, vol. 69, no. 1, pp. 619–633, Jan. 2021.

[37] Y. Zheng, S. Bi, Y.-J. A. Zhang, X. Lin, and H. Wang, "Joint Beamforming and Power Control for Throughput Maximization in IRS-Assisted MISO WPCNs," *IEEE Internet Things J.*, vol. 8, no. 10, pp. 8399–8410, Aug. 2021.

[38] Q. Wu, X. Zhou, and R. Schober, "IRS-Assisted Wireless Powered NOMA: Do We Really Need Different Phase Shifts in DL and UL?" *IEEE Wireless Commun. Lett.*, vol. 10, no. 7, pp. 1493–1497, Jul. 2021.

[39] Q. Wu, X. Zhou, W. Chen, J. Li, and X. Zhang, "IRS-Aided WPCNs: A New Optimization Framework for Dynamic IRS Beamforming," *IEEE Trans. Wireless Commun.*, vol. 21, no. 7, pp. 4725–4739, Jul. 2022.

[40] Z. Chu, P. Xiao, M. Shojafar, D. Mi, J. Mao, and W. Hao, "Intelligent Reflecting Surface Assisted Mobile Edge Computing for Internet of Things," *IEEE Wireless Commun. Lett.*, vol. 10, no. 3, pp. 619–623, Jun. 2021.

[41] T. Bai, C. Pan, Y. Deng, M. Elkashlan, A. Nallanathan, and L. Hanzo, "Latency Minimization for Intelligent Reflecting Surface Aided Mobile Edge Computing," *IEEE J. Sel. Areas Commun.*, vol. 38, no. 11, pp. 2666–2682, Nov. 2020.

[42] H. Ju and R. Zhang, "Throughput Maximization in Wireless Powered Communication Networks," *IEEE Trans. Wireless Commun.*, vol. 13, no. 1, pp. 418–428, Jan. 2014.

[43] S. Boyd and L. Vandenberghe, *Convex Optimization*. Cambridge, U.K.: Cambridge Univ. Press, 2004.

Guangji Chen received the Ph.D degree in information and communication engineering from the University of Science and Technology of China (USTC), Hefei, China, in 2020. From 2020 to 2021, he was a Senior Engineer at Huawei Technologies Company Ltd., Nanjing, China. He is currently a Post-Doctoral Researcher in the State Key Laboratory of Internet of Things for Smart City, University of Macau, Macau, China.

His current research interests include intelligent reflecting surface (IRS), non-orthogonal multiple access, ultra dense network (UDN), and stochastic geometry.

Qingqing Wu (S'13-M'16-SM'21) received the B.Eng. and the Ph.D. degrees in Electronic Engineering from South China University of Technology and Shanghai Jiao Tong University (SJTU) in 2012 and 2016, respectively. He is currently an assistant professor with the State key laboratory of Internet of Things for Smart City, University of Macau. From 2016 to 2020, he was a Research Fellow in the Department of Electrical and Computer Engineering at National University of Singapore. His current research interest includes intelligent reflecting surface (IRS), unmanned aerial vehicle (UAV) communications, and MIMO transceiver design. He has coauthored more than 100 IEEE journal papers with 25 ESI highly cited papers and 8 ESI hot papers, which have received more than 13,000 Google citations. He was listed as the Clarivate ESI Highly Cited Researcher in 2021, the Most Influential Scholar Award in AI-2000 by Aminer in 2021 and Worlds Top 2% Scientist by Stanford University in 2020 and 2021.

He was the recipient of the IEEE Communications Society Young Author Best Paper Award in 2021, the Outstanding Ph.D. Thesis Award of China Institute of Communications in 2017, the Outstanding Ph.D. Thesis Funding in SJTU in 2016, the IEEE ICCC Best Paper Award in 2021, and IEEE WCSP Best Paper Award in 2015. He was the Exemplary Editor of IEEE Communications Letters in 2019 and the Exemplary Reviewer of several IEEE journals. He serves as an Associate Editor for IEEE Transactions on Communications, IEEE Communications Letters, IEEE Wireless Communications Letters, IEEE Open Journal of Communications Society (OJ-COMS), and IEEE Open Journal of Vehicular Technology (OJVT). He is the Lead Guest Editor for IEEE Journal on Selected Areas in Communications on "UAV Communications in 5G and Beyond Networks", and the Guest Editor for IEEE OJVT on 6G Intelligent Communications" and IEEE OJ-COMS on Reconfigurable Intelligent Surface-Based Communications for 6G Wireless Networks". He is the workshop co-chair for IEEE ICC 2019-2022 workshop on Integrating UAVs into 5G and Beyond, and the workshop co-chair for IEEE GLOBECOM 2020 and ICC 2021 workshop on Reconfigurable Intelligent Surfaces for Wireless Communication for Beyond 5G. He serves as the Workshops and Symposia Officer of Reconfigurable Intelligent Surfaces Emerging Technology Initiative and Research Blog Officer of Aerial Communications Emerging Technology Initiative. He is the IEEE Communications Society Young Professional Chair in Asia Pacific Region.

Wen Chen (M'03-SM'11) is a tenured Professor with the Department of Electronic Engineering, Shanghai Jiao Tong University, China, where he is the director of Broadband Access Network Laboratory. He is a fellow of Chinese Institute of Electronics and the distinguished lecturers of IEEE Communications Society and IEEE Vehicular Technology Society. He is the Shanghai Chapter Chair of IEEE Vehicular Technology Society, Editors of IEEE Transactions on Wireless Communications, IEEE Transactions on Communications, IEEE Access and IEEE Open Journal of Vehicular Technology. His research interests include multiple access, wireless AI and meta-surface communications. He has published more than 110 papers in IEEE journals and more than 120 papers in IEEE Conferences, with citations more than 8000 in google scholar.

Derrick Wing Kwan Ng (S'06-M'12-SM'17-F'21) received a bachelor's degree with first-class honors and a Master of Philosophy (M.Phil.) degree in electronic engineering from the Hong Kong University of Science and Technology (HKUST) in 2006 and 2008, respectively. He received his Ph.D. degree from the University of British Columbia (UBC) in Nov. 2012. He was a senior postdoctoral fellow at the Institute for Digital Communications, Friedrich-Alexander-University Erlangen-Nürnberg (FAU), Germany. He is now working as a Scientia Associate Professor at the University of New South Wales, Sydney, Australia. His research interests include global optimization, physical layer security, IRS-assisted communication, UAV-assisted communication, wireless information and power transfer, and green (energy-efficient) wireless communications.

Dr. Ng has been listed as a Highly Cited Researcher by Clarivate Analytics (Web of Science) since 2018. He received the Australian Research Council (ARC) Discovery Early Career Researcher Award 2017, the IEEE Communications Society Stephen O. Rice Prize 2022, the Best Paper Awards at the WCSP 2020, 2021, IEEE TCGCC Best Journal Paper Award 2018, INISCOM 2018, IEEE International Conference on Communications (ICC) 2018, 2021, IEEE International Conference on Computing, Networking and Communications (ICNC) 2016, IEEE Wireless Communications and Networking Conference (WCNC) 2012, the IEEE Global Telecommunication Conference (Globecom) 2011, 2021 and the IEEE Third International Conference on Communications and Networking in China 2008. He served as an editorial assistant to the Editor-in-Chief of the IEEE Transactions on Communications from Jan. 2012 to Dec. 2019. He is now serving as an editor for the IEEE Transactions on Communications, the IEEE Transactions on Wireless Communications, and an Associate Editor-in-Chief for the IEEE Open Journal of the Communications Society.

Lajos Hanzo (http://www-mobile.ecs.soton.ac.uk, https://en.wikipedia.org/wiki/Lajos_Hanzo)

(FIEEE'04) received his Master degree and Doctorate in 1976 and 1983, respectively from the Technical University (TU) of Budapest. He was also awarded the Doctor of Sciences (DSc) degree by the University of Southampton (2004) and Honorary Doctorates by the TU of Budapest (2009) and by the University of Edinburgh (2015). He is a Foreign Member of the Hungarian Academy of Sciences and a former Editor-in-Chief of the IEEE Press. He has served several terms as Governor of both IEEE ComSoc and of VTS. He has published 2000+ contributions at IEEE Xplore, 19 Wiley-IEEE Press books and has helped the fast-track career of 123 PhD students. Over 40 of them are Professors at various stages of their careers in academia and many of them are leading scientists in the wireless industry. He is also a Fellow of the Royal Academy of Engineering (FREng), of the IET and of EURASIP. He holds the Eric Sumner Field Award.